TÜBİTAK

Turkish Journal of Earth Sciences

http://journals.tubitak.gov.tr/earth/

Research Article

Turkish J Earth Sci
(2019) 28: 760-785

doi:10.3906/yer-1812-8

The mineralogical and geochemical composition of Holocene sediments from Lake Hazar, Elazığ, Eastern Turkey: implications for weathering, paleoclimate, redox conditions, provenance, and tectonic setting

Dicle BAL AKKOCA[1,*], K. Kadir ERİŞ[2], M. Namık ÇAĞATAY[2], Demet BİLTEKİN[3]

[1]Department of Geological Engineering, Faculty of Engineering, Fırat University, Elazığ, Turkey

[2]Department of Geological Engineering, Eastern Mediterranean Centre for Oceanography and Limnology and Faculty of Mines, İstanbul Technical University, Maslak, İstanbul, Turkey

[3]Department of Marine Sciences Technology Engineering, Fatsa Faculty of Marine Sciences, Ordu University, Fatsa, Ordu, Turkey

Received: 18.12.2018 • **Accepted/Published Online:** 29.07.2019 • **Final Version:** 04.09.2019

Abstract: Mineralogical and geochemical analyses of samples collected from piston core HZ11-P01 at the western margin of Lake Hazar were studied to determine the provenance and weathering conditions on the source area together with tectonic setting of the source rocks, paleoclimate of the region, and paleo-redox conditions of the lake sediments. Nonclay minerals in the sediment core are represented by feldspar, quartz, dolomite, and calcite. The clay mineral assemblage consists of smectite/chlorite mixed-layer clay, chlorite, and illite. Most major, trace, and rare earth element contents of the lake samples are generally similar to those of the catchment area. Chondrite-normalized rare earth element patterns of the lake samples are characterized by enrichment of light rare earth elements, a relatively flat heavy rare earth element pattern, and no Eu negative anomaly. The chemical index of alteration and index of compositional variability of the core sediment suggested that the intensity of weathering in the source area was low to moderate. The paleoclimatic indicator (C-values) showed that a paleoclimate changing from semiarid to semimoist prevailed during the last ~2 ka BP. Authigenic U and element ratios such as Th/U, Ni/Co, Cu/Zn, V/Cr, Eu/Eu*, and Ce/Ce* indicate that the lake sediments were deposited under oxic conditions. La/Sc, Co/Th, Cr/Th, Zr/Sc, and Th/Sc element ratios in the core sediments are consistent with values of sediments derived from mainly mafic and intermediate source rocks. According to discriminant-function diagrams, lake samples are plotted within the arc setting and arc-continent collision, which is in accordance with the geology of the study area.

Key words: Chemical index of alteration, redox conditions, provenance, tectonic setting, Lake Hazar, Eastern Turkey

1. Introduction

The mineralogical and chemical compositions of lake sediments are mainly controlled by the properties of the sedimentary environment. They are also preferentially affected by several factors such as source rock, catchment weathering, tectonic setting of the source rocks, and paleoclimate of the region (Yuretich et al., 1999; Condie et al., 2001; Wanas and Abdel-Maguid, 2006; Hseu et al., 2007; Alizai et al., 2012; Armstrong-Altrin et al., 2013; Tao et al., 2013; Song et al., 2014; Armstrong-Altrin, 2015; Garzanti et al., 2016; Huvaj and Huff, 2016; Şengün and Koralay, 2019). Although sedimentological and tectonic records are available for several sedimentary basins in Eastern Turkey, studies regarding geochemical characteristics of these basins are very limited (Eker and Korkmaz, 2011; Tetiker, 2014; Akkoca and Işık, 2018).

Lake Hazar is situated on the Eastern Anatolian Fault Zone (EAFZ) (Figures 1a and 1b), having a maximum depth of 220 m (Eriş, 2013). The lake covers an area of 78.44 km^2 and has a volume of 7.5×10^9 m^3. The lake has a closed drainage system that is mainly discharged by the Kürkçayı and Zıkkım rivers from the western and eastern margins. On the other hand, there are several permanent inlets and ephemeral creeks that drain the northern and southern catchments, providing water and clastic sediments to the lake (Figure 1b).

Different models have been proposed for the evolution of the Hazar Basin and its current relationship to the EAFZ (Hempton et al., 1983; Aksoy et al., 2007; Khalifa et al., 2018). However, the recent interpretation of Garcia-Moreno et al. (2010) based on the relationships of various morphotectonic structures along the lake floor proposed that Lake Hazar Basin is a pull-apart basin. In their study, the structure of the basin was examined by utilizing a bathymetric map and seismic profiles together with the sediment core.

* Correspondence: dbal@firat.edu.tr

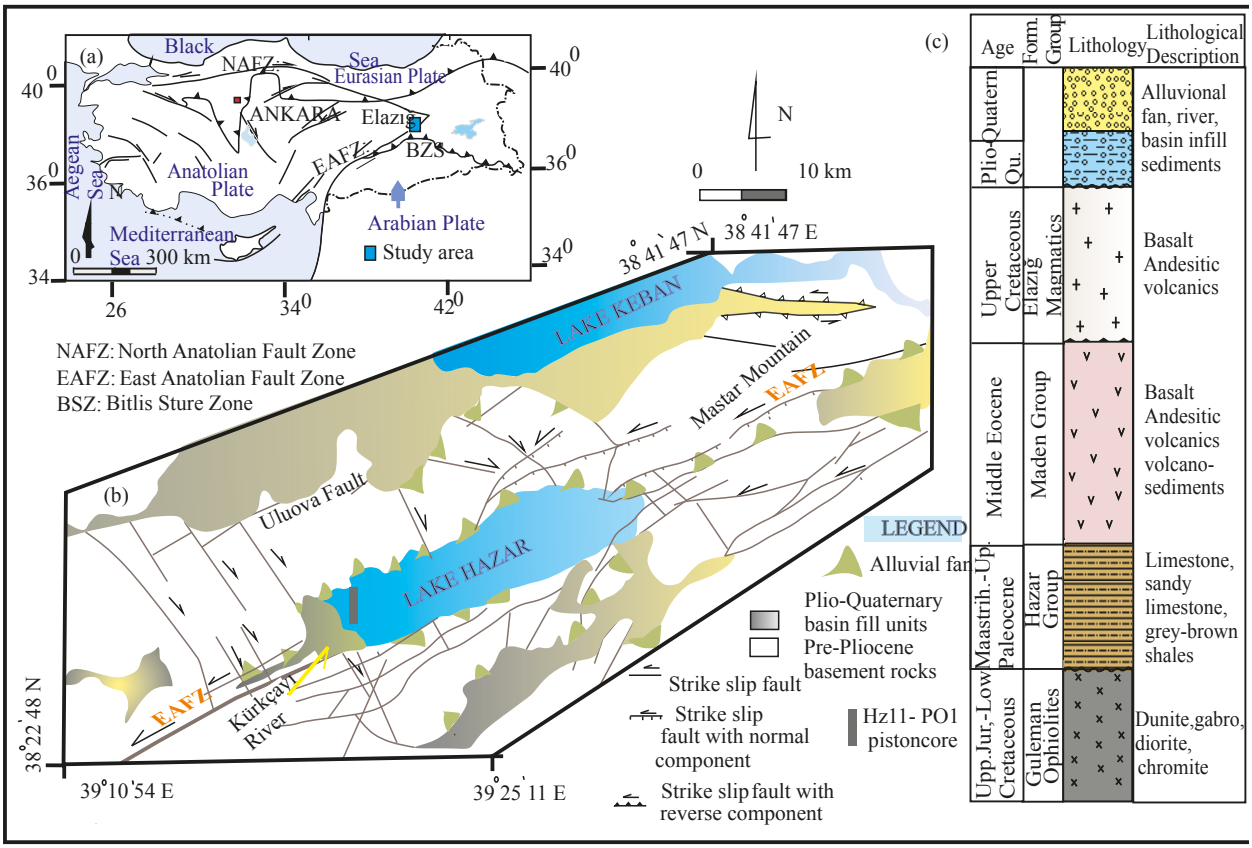

Figure 1. (a) Simplified map showing the location of Lake Hazar in eastern Turkey. (b) Simplified map of Lake Hazar Basin, Kürkçayı, and fault-parallel alluvial fans (modified from Aksoy et al., 2007). (c) Tectono-stratigraphic columnar section showing lithostratigraphic units of Lake Hazar (from Çelik, 2003).

Eriş (2013) and Eriş et al. (2018a) studied high-resolution seismic reflection profiles and sediment cores from Lake Hazar and documented a detailed record of lake-level fluctuations and a robust chronology of paleoclimatic changes in the Eastern Anatolia during the late Pleistocene to Holocene. A different approach for extracting paleoclimate proxies, namely independent component analysis, was proposed by Ön et al. (2017) and provided a high-resolution paleoclimate record of Lake Hazar through the late Pleistocene to Holocene. Eriş et al. (2018b) studied the effects of climate and tectonic interactions in the lake sediments spanning the middle to late Holocene and documented remarkable tectonic markers that controlled the depositional conditions. High-resolution seismic data, magnetic susceptibility, total organic carbon, and Ca, Fe, K, Mn, Sr, and Ti element contents were used in these previous studies. The paleoclimate reconstruction was also supported by a high-resolution pollen analysis by Biltekin et al. (2018), who presented the evolution of paleovegetation with respect to climate changes. On the other hand, rather than the elemental profiles investigated in previous studies, other major oxide, trace, and rare earth element (REE) contents of Lake Hazar sediments have not yet been studied. For this purpose, we examined piston core HZ11-P01 recovered from a well close to the mouth of the Kürkçayı River and alluvial fans that flow into the western depression of the lake. Our main objective is to discuss chemical weathering in the catchment area, the paleoclimate of the region, redox conditions at the sediment/water interface of the lake, the provenance of the lake sediments, and the tectonic setting of the source rocks in the catchment by using mineralogical and geochemical composition of the lake sediments during the last ~2 ka BP.

2. Geological setting

Lake Hazar is a 25-km-long, 7-km-wide strike-slip sedimentary basin with a north-eastern trending elongated-shape on the EAFZ (Figures 1a and 1b). The basin has been described as an active pull-apart basin (Şengör et al., 1985; Çetin et al., 2003). In the Quaternary, the western part of the lake was discharged by the Kürkçayı River and alluvial fans of diverse size extending parallel to the fault (Aksoy et al., 2007; Eriş et al., 2018a) (Figure 1b). The main geological units in the studied area are upper Jurassic-

lower Cretaceous Guleman ophiolites, upper Cretaceous Elazığ magmatics, the Maastrichtian-upper Paleocene Hazar Group, the middle Eocene Maden Group, and Plio-Quaternary and Quaternary alluviums. Outcrops of the Elazığ magmatics and the Maden Group can be observed around the Kürkçayı River and in the vicinity of alluvial fans at the western part of the lake (Figures 1c and 2).

The Guleman ophiolites, consisting of harzburgite, dunite lenses, and podiform chromitites, are located at the eastern part of the lake (Figure 2). Bingöl (1986) suggested that this unit was formed in a midoceanic ridge. The Elazığ magmatics are located at the western part of the lake (Figure 2) and comprise basaltic, andesitic lava flows (Ural et al., 2015). The Elazığ magmatics belong to a calc-alkaline series of island-arc magmatism and arc-continent collision (Yazgan and Chessex, 1991; Robertson et al., 2007). The Hazar Group is located at the eastern part of the lake (Figure 2) and consists of conglomerates changing laterally and vertically to limestone and shales. According to Çelik (2003), this formation was deposited in a shallow marine environment. The Maden Group is exposed west of the Kürkçayı River and to the northeast of Lake Hazar. It contains basalts, basaltic andesites, andesitic volcanics, and volcanosediments around the lake (Erdem, 1987). Bozkaya et al. (2006) proposed that the Maden Group rocks are products of a back-arc volcanism. Ertürk et al. (2018) found new evidence to suggest a postcollisional magmatism for the tectonic setting of these rocks.

3. Materials and methods

The studied core, HZ11-PO1, was recovered at a water depth of 48 m at 38°27′54″N, 39°18′59″E by a percussion piston corer of 7.5 cm in diameter. The core, 2.2 m in length, was transported to the refrigerated (4 °C) core repository in the Geology Department of Fırat University. ^{14}C dating of core material was carried out at the Woods Hole NOSAMS on selected mollusk shells that had been carefully cleaned and examined under a microscope to ensure that they were diagenetically unaltered. The radiocarbon ages (^{14}C ka BP) are reported without reservoir correction (Siani et al., 2000) and without calibration according to Stuiver and Reimer (1993).

X-ray studies of the lake samples were carried out with the Rigaku DMAXIII diffractometer using Ni-filtered Cu Kα at 15 kV-40 mA instrumental settings. Bulk mineral compositions of 40 lake samples and clay mineral compositions of 20 lake samples were determined. The bulk mineralogy was determined by X-ray powder

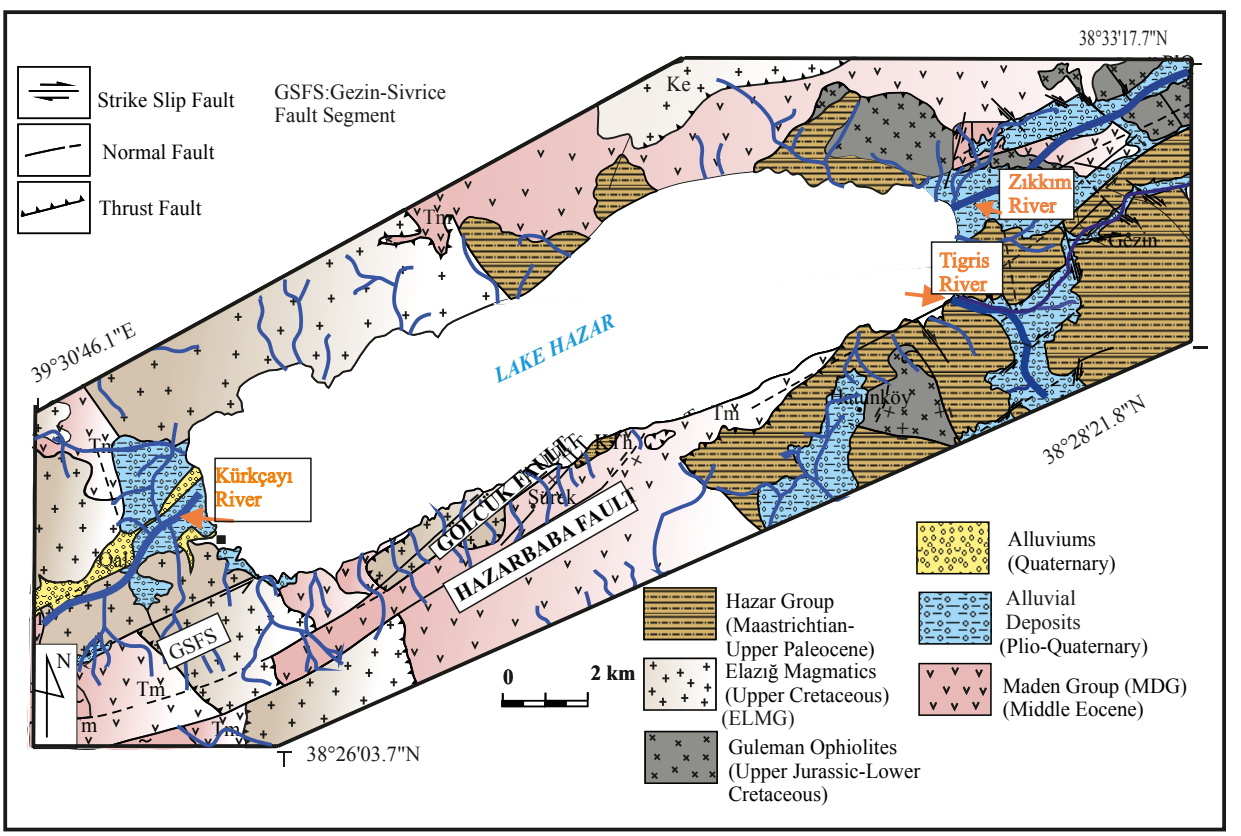

Figure 2. Geology map of the study area (modified from Gürocak, 1993).

diffraction (XRD). The clay fraction was separated according to the principles of Stoke's law (Folk, 1974). Clay mineralogy was determined by XRD using oriented samples after air-drying, saturation with ethylene glycol for 12 h, and heating at 490 °C for 4 h. The whole-rock and clay mineral percentages were determined following the intensity constants of Temel and Gündoğdu (1996) after Brindley (1980). In this method, all samples were mounted in random and oriented mounts. The characteristic peak intensities (I) of minerals were normalized to that of the (104) reflection of dolomite. Accordingly, the areas of the air-dried 3.04-Å peak were multiplied by 0.74 to yield calcite, the area of the 3.34-Å peak was multiplied by 0.34 to obtain quartz, the 3.20-Å peak areas were multiplied by 1.62 to estimate feldspar, and the 4.48-Å peak areas were multiplied by 14.63 to yield clay minerals. Clay minerals were estimated by weighting the integrated peak areas of characteristic basal reflections in the glycolated state with the empirical factors of Temel and Gündoğdu (1996) after Brindley (1980). Characteristic peak intensities (I) of the minerals were normalized to that of the (104) reflection of dolomite. Accordingly, the areas of the glycolated 5.7-Å peak were multiplied by 0.51 to obtain illite, the 7.8-Å peak areas were multiplied by 0.83 to yield smectite/chlorite (S-C), and the 5.4-Å peak areas were multiplied by 0.83 to yield chlorite (C) contents. The relative accuracy of this method is within 15%. As a consequence of these mineralogical studies, the types of bedrock and clay mineral assemblage of core sediments were determined, and the results are discussed with respect to geochemical findings.

Scanning electron microscopy (SEM) was used for three lake samples to observe the morphology and shape of the clay minerals in different levels of the piston core. A Zeiss EVO MA10 scanning electron microscope instrument with energy-dispersive X-ray (EDX) capabilities was used.

In order to compare geochemical characteristics of bedrocks and piston core samples, 5 samples were collected from the Elazığ magmatics (labeled ELM1) at the west side of the lake and another 5 samples were taken from the Maden Group (labeled MDG1). These samples and 20 samples from the HZ11-P01 piston core were analyzed at Acme Analytical Laboratories Ltd. (Canada) for major, trace, and REE contents. Elements were measured on glass pellets that were produced in a platinum-gold crucible by adding a 1/5 ratio of sample and lithium tetraborate ($Li_2B_4O_7$) at 1150 °C. Moreover, the average of 15 samples from the Elazığ magmatics outcropping at the northeast of Lake Hazar was labeled ELM2, which were compiled from the study of Dönmez (2006). Likewise, the average of 8 samples from the Maden Group rocks to the southeast of Lake Hazar was labeled MDG2, which were compiled by Ertürk et al. (2018).

4. Results

4.1. Sedimentology and stratigraphy of the core

The HZ11-P01 piston core, 2 m in length, covers the last ~2 ka ^{14}C ka BP on the basis of uncalibrated ^{14}C ages (Figure 3). AMS ^{14}C analysis of a mollusk shell close to the lowermost part of the core suggested an age of 1730 ^{14}C ka BP. The core begins at its lowermost part with alternations of dark and light gray homogeneous clays that terminate at 1.72 m with a yellowish green silty clay layer. Upward in the core, between 1.72 and 1 m, light gray silty clay and green gray homogeneous clay are intercalated by thin layers of silty clay. The most remarkable change in the core occurs at 0.76 m, where the homogeneous clay passes upward into alternations of dark and light gray mud with silty clay layers and homogeneous clay intercalation. AMS ^{14}C ka BP analysis of an ostracod shell from the upper part of the unit indicates an age of 885 ^{14}C ka BP (Figure 3). In the upper part of the core, between 0.38 m and 0.21

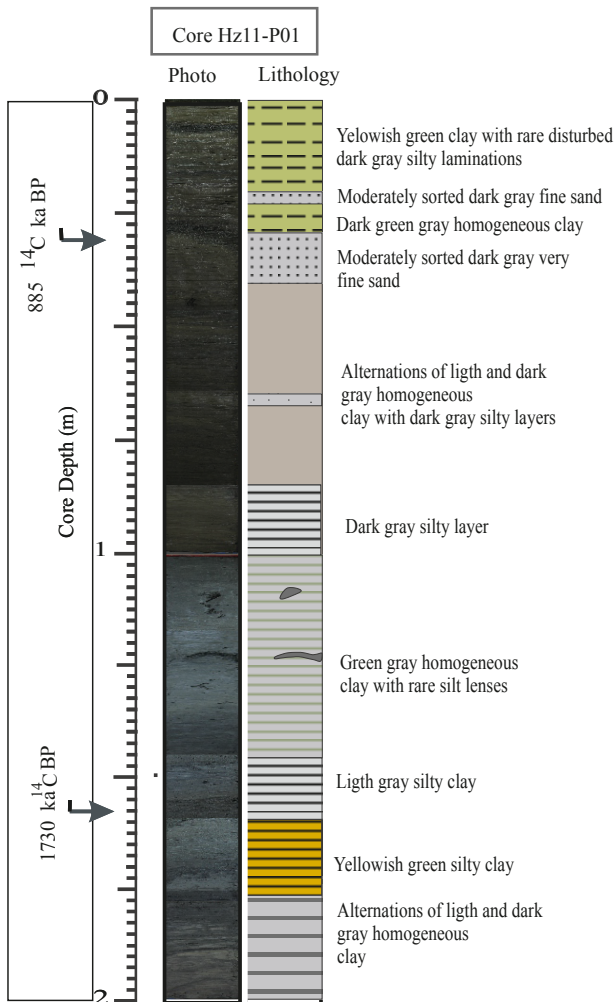

Figure 3. Lithostratigraphic definition of studied piston-core HZ11-P01.

m, moderately sorted, very fine sand layers alternate with dark gray homogeneous clay. The core sequence in the uppermost 0.21 m consists of yellowish green clay with some disturbed silty laminations.

4.2. Mineralogical composition

Whole-rock XRD patterns of samples P0105 and P0160 from different levels are shown in Figure 4a. In whole-rock XRD analysis, mean peaks of clay 4.47 Å (2θ = 19°), quartz 3.34 Å (2θ = 26°), feldspar 3.20 Å (2θ = 28°), dolomite 2.90 Å (2θ = 31°), and calcite 3.03 Å (2θ = 30°) were identified (Figures 4a and 4b). The whole-rock mineral assemblage of lake sediments consists of 45% to 79% clay, 10% to 32% feldspars, 7% to 16% quartz, 1% to 10% dolomite, and 1% to 7% calcite (Table 1).

In clay fraction XRD patterns, illite peaks of 10.13, 5.03, and 3.35 Å did not change with glycolation and heating. The characteristic peaks of chlorite are 14.2, 7.01, and 4.7 Å and these remain similar in the air-dried and glycolated XRD patterns shown in Figure 4b. The intensity of the 7.01-Å peak decreases in heated samples. The peak at 7.8 Å in air-dried patterns of smectite/chlorite mixed-layer clay is wider and broader than those of chlorite. The characteristic peaks of S-C are 14.01, 9.3, and 7.8 Å. Specifically, a characteristic peak of S-C shifted from 14.01 to 15.5 Å after ethylene glycol saturation and then collapsed to 12.04 Å with heating (Figures 4c and 4d). The clay minerals in these samples from core HZ11-P01 range from 24% to 55% smectite/chlorite mixed-layer clay, 22% to 42% chlorite, and 17% to 38% illite (Table 1).

4.3. SEM analyses

Results of SEM and EDX analyses of samples P05, P0175, and P0195 that represent different depths and lithological levels of lake sediments are shown in Figures 5a–5c. In sample P05 the most abundant clay mineral is chlorite (Figure 5a). Chlorite is characterized by lath-shaped plates with crystal thickness of 2–6 μm (Figure 5a). Smectite-chlorite flakes coat the surface of glassy volcanic fragments and appear in the form of flake-shaped spongy hyaloclasts in sample P0175 (Figure 5b). Illites are observed as stick-like particles in sample P0195 (Figure 5c). The morphology

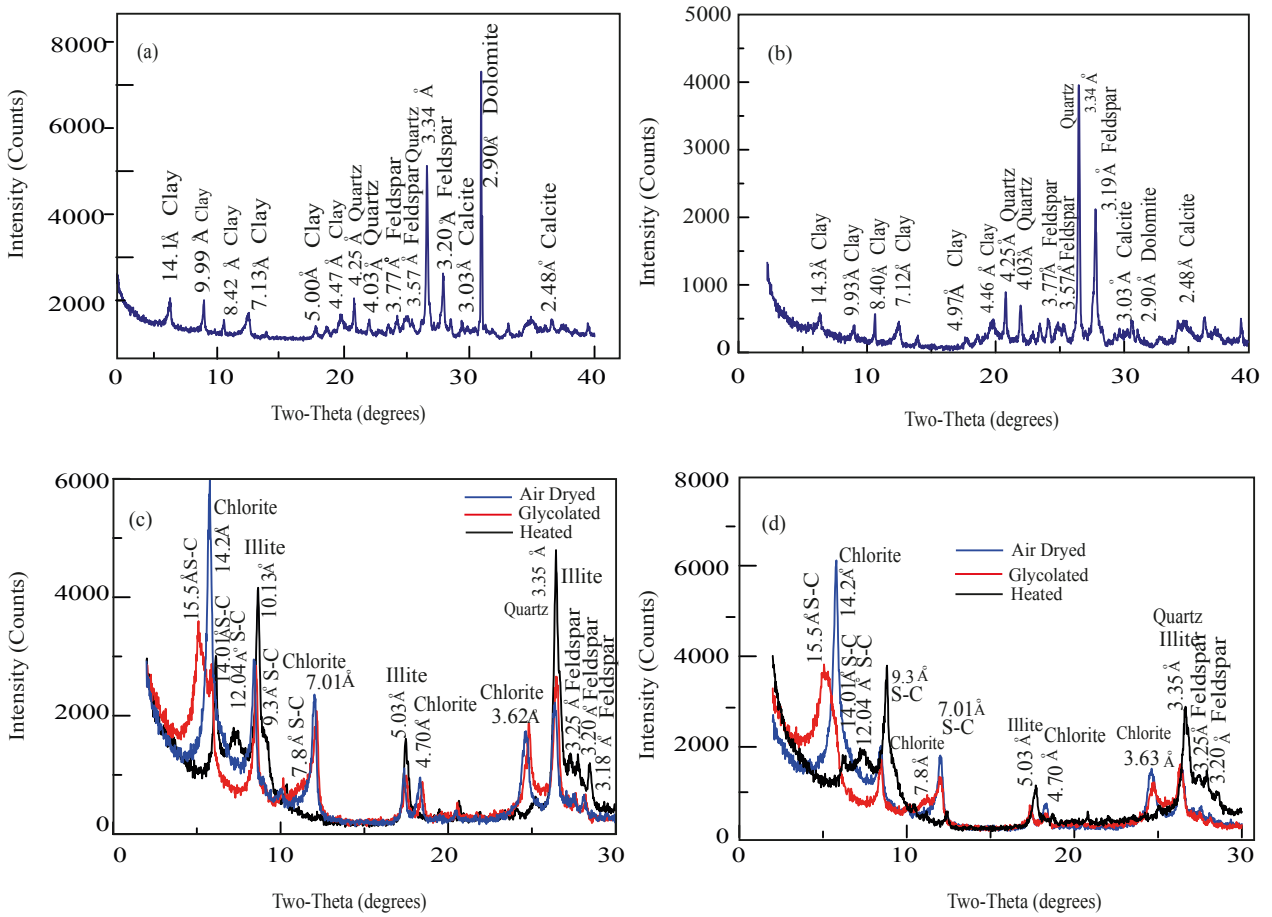

Figure 4. X-ray diffraction (XRD) patterns of (a) P0100 and (b) P0160 samples. Clay fraction XRD patterns of (c) P0100 and (d) P0160 samples.

Table 1. Mean, standard deviation, and coefficient of variation (CV = standard deviation / mean × 100) of the semiquantitative relative whole-rock (n = 40) mineral fraction and clay mineral fraction (n = 20) abundance (%) of the lake samples. S-C: Smectite-chlorite mixed-layer clays.

	Whole-rock mineral (%) (n = 40)					Clay minerals (%) (n = 20)		
	Clay	Feldspar	Quartz	Dolomite	Calcite	Chlorite	S-C	Illite
Mean	65	18.85	9.125	3.6	2.5	33.05	41.85	24.6
Maximum	79	32	16	10	7.0	42	55	38
Minimum	45	10	7.0	1.0	1.0	22	24	17
Standard deviation	7.37	5.09	1.77	1.66	1.46	5.87	7.56	5.66
Coefficient of variation	11.19	27.03	19.41	46.13	58.7	13.9	13.7	14.8

of clays displayed thick plates and rounded outlines and they did not show a significant change in these three samples (Figure 5). EDX data from these samples indicate that all clays mainly contain O, Mg, Al, Si, and K elements; however, Fe and Mg contents are high in chlorite and differently from other minerals S-C contains Ti (Figures 5a and 5b). Illite is represented by low Fe and Mg and high K concentrations (Figure 5c).

4.4. Geochemistry

4.4.1. Major and trace elements

Major and trace element concentrations of bedrocks (Elazığ magmatics, ELM1–2; Maden Group, MDG1–2) and lake samples are shown in Tables 2a and 2b. Average data of the Post-Archean Australian shales (PAAS) of Taylor and McLennan (1985), which are considered to represent the upper continental crust composition, are included as a reference. Compositional variations of the lake samples are comparatively low. The average concentrations of SiO_2, Al_2O_3, Fe_2O_3, and MgO in the lake samples are 46.83 wt.%, 15.35 wt.%, 8.58 wt.%, and 5.40 wt.%, respectively.

The correlation between the major elements and Al_2O_3 is shown in Figure 6a. The lack of a significant positive correlation between SiO_2 and Al_2O_3 is due to the fact that most of the silica is sequestered in quartz (Rahman and Suzuki, 2007). Positive correlation of TiO_2 with Al_2O_3 suggests that TiO_2 is probably associated with silicates and phyllosilicates, especially with illite (Dabard, 1990). The positive correlation of Fe_2O_3, MgO, P_2O_5, and MnO with Al_2O_3 suggests that their distribution is mainly controlled by silicates and phyllosilicates (Dabard, 1990; Rahman and Suzuki, 2007; Descourvieres et al., 2011).

Major oxides are normalized with PAAS values (Taylor and McLennan, 1985) (Figure 6b). CaO and MgO show 5.44- and 2.46-fold enrichments with respect to PAAS, which is attributed to the presence of diagenetic calcite and dolomite cements. The results of XRD analysis revealed the presence of calcite and dolomite (Figures 4a and 4b; Table 1). Felsic rocks contain a high amount of K (Wedepohl, 1978). K_2O shows depletion with respect to PAAS (0.42 × PAAS), indicating that the source rock of the studied samples is not felsic continental source rock, like PAAS (Figure 6b).

In the Herron (1988) diagram, the lake samples are classified as Fe-shale and their geochemical composition is not consistent with upper continental crust (UCC), PAAS, or North American shale composite (NASC) (Figure 6c). The Fe-shale character of samples might indicate that source rocks have a composition that varies from intermediate to mafic (Roser and Korch, 1986). The geochemical characteristics of lake samples are quite similar to those of surrounding rocks (ELM1–2 and MDG1–2) along the Kürkçayı River route and alluvial fans at the western margin of Lake Hazar. Na_2O contents of lake samples are lower than those of samples ELM1–2 and MDG1–2 (average in lake samples, 1.66; in ELM1–2, 3.95–4.26; in MDG, 3.25, 3.85) (Tables 2a and 2b; Figure 6b). Na is easily removed during chemical weathering (Ling et al., 2013). Therefore, lower contents of Na_2O must be due to the weathering of lake sediments.

Figure 7a illustrates the correlation of Al_2O_3 with trace elements. The high correlation of trace elements (e.g., Ni, V, Rb, Ba, Pb, Zr, Nb, Th, U, Cu, Sc, Zn, Co) with Al_2O_3 (Pearson correlation coefficients between 0.58 and 0.91) suggests that these elements may be bound in clay minerals and feldspar during weathering (Fedo et al., 1996; Nagarajan et al., 2007). Slightly lower positive correlations of Cr, Y, and Hf with Al_2O_3 (with respective r values of 0.45, 0.31, and 0.39) may result from different source regions for these elements. Cr may be linked with clinopyroxenes and opaque minerals, while Y and Hf might be associated with heavy minerals (Craigie, 2018). Sr is significantly negatively correlated with Al_2O_3 ($r = -0.92$) since Sr is generally bound to carbonate minerals (Dix, 2006).

Selected trace elements are normalized with PAAS (Taylor and McLennan, 1985) (Figure 7b). As shown Figure 7, lake samples are depleted in Th, Ba, Rb, and U

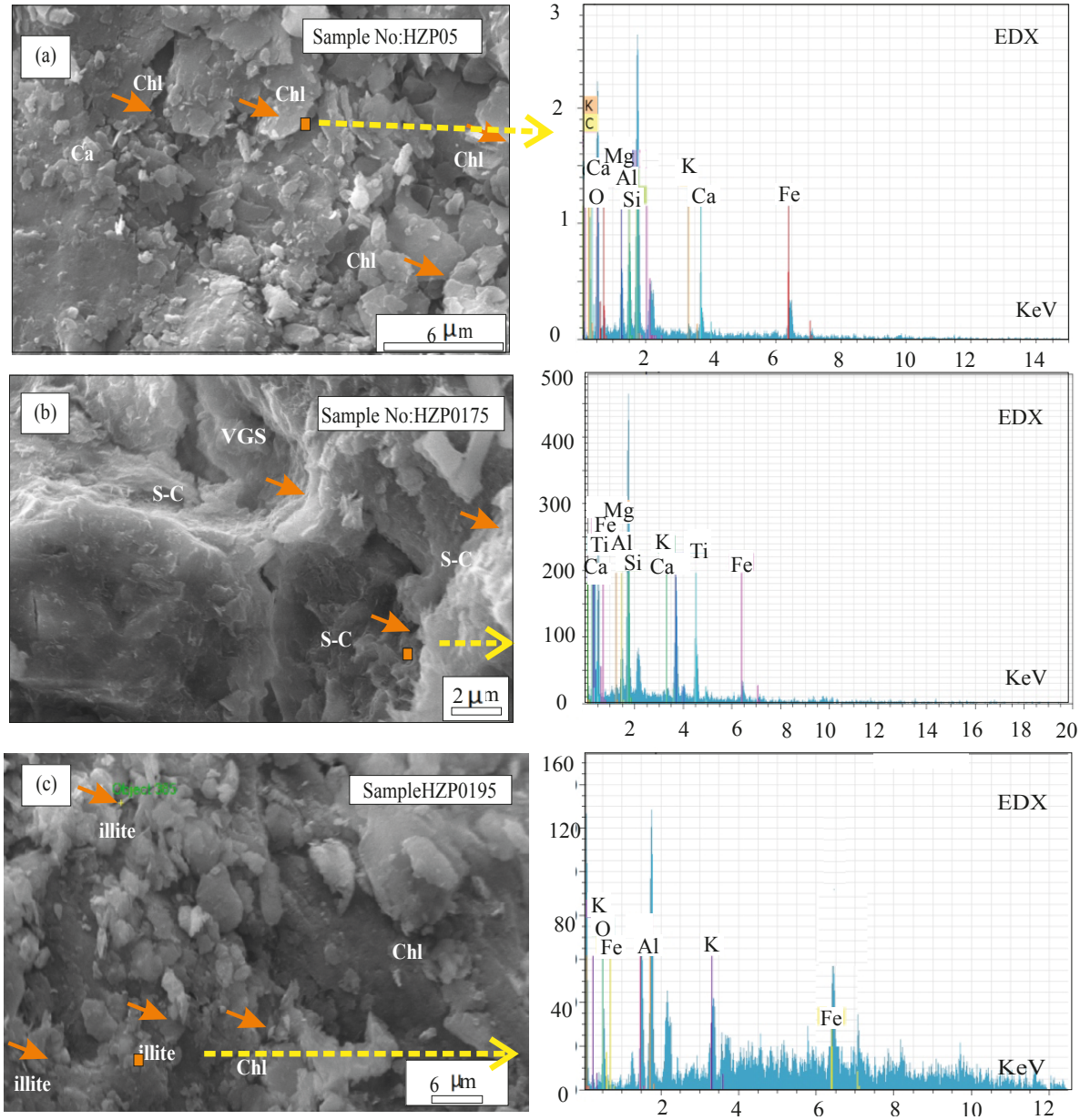

Figure 5. Scanning electron microscopy (SEM) photos and energy dispersion spectrometer (EDX) analysis of marked patch of samples. (a) Chlorites (Chl), which are characterized by lath-shaped plates with crystal thickness of 2–6 µm, calcite (Ca) (sample P05). (b) Spongy hyaloclasts, authigenic forms of smectite-chlorite (S-C) (sample P0175). VGS: Volcanic glass shards. (c) Stick-shaped illite particles (sample P0195) and chlorites (Chl).

but enriched in transition elements of Ni, Cr, Sc, V, Co, and Cu, and this might indicate that all samples are less acidic with respect to PAAS of crustal origin. Concentrations of immobile elements (e.g., Sc, Zr, Hf, Y) of lake samples are similar to those of ELM1–2 and MDG1–2. The fact that concentrations of Ba, Rb, and Pb in lake sediments are higher than those of ELM1–2 and MDG1–2 bedrock samples is attributed to adsorption of these elements on the clay surface (Uddin, 2017). Variations of U contents in lake samples relative to ELM1–2 and MDG1–2 can be related to redox conditions in the lake as U is a redox-sensitive element (Martinez-Ruiz et al., 2015). The Sr content of lake samples is higher than that of ELM1–2 and MDG1–2, which could be due to its retention within the carbonate minerals (Figure 7b).

4.4.2. Rare earth elements (REEs)

The concentrations of REEs in samples ELM1–2 MDG1–2 and lake samples are listed in Tables 3a and 3b. The PAAS

Table 2. Major trace elements and some element ratios of (a) surrounding rocks, Elazığ magmatics (ELM1: this study), Maden Group (MDG1: this study), ELM2 (from Dönmez, 2006, n = 15), MDG2 (from Ertürk et al., 2018, n = 8). (b) Lake samples, Post-Archean Australian shales (PAAS) (from Taylor and McLennan, 1985). Fe_2O_3*: Total Fe; LOI: loss of ignition at 1050 °C; CIA* = 10 × [Al_2O_3 / (Al_2O_3 + CaO* + Na_2O + K_2O)]. (CIW = Al_2O_3 / (Al_2O_3 + CaO* + Na_2O) × 100). The molar proportion of Na_2O is taken as the molar proportion of CaO from the silicate fraction according to the indirect method of McLennan et al. (1993). Authigenic (U) = (totalU) – Th / 3 (Martinez-Ruiz et al., 2015). ICV = [Fe_2O_3 + K_2O + Na_2O + CaO + MgO + TiO_2 / Al_2O_3]; C-value = [Σ(Fe + Mn + Cr + Ni + V + Co) / Σ (Ca + Mg + Sr + Ba + K + Na)] (Zhao et al., 2007).

Table 2a.

					Surrounding rocks									
Elements (%)			ELM1					MDG1						
	HE1	HE2	HE3	HE4	HE5	Average	HM1	HM2	HM3	HM4	HM5	Average	ELM2	MDG2
SiO_2	58.3	59.42	64.7	59.15	59.8	60.27	51.79	51.36	43.63	51.24	51.99	50.0	55.9	51.17
Al_2O_3	16.52	15.89	15.84	16.99	16.14	16.27	20.23	22.12	17.28	17.14	17.07	18.76	14.86	16.96
Fe_2O_3	6.32	6.2	4.63	6.31	5.85	5.86	10.96	10.22	9.88	8.99	8.31	9.67	7.43	8.78
MgO	3.48	3.38	1.78	2.67	3.08	2.87	2.29	2.13	6.28	4.35	3.04	3.61	4.51	5.83
CaO	4.52	4.75	2.64	3.73	6.26	4.38	4.37	3.43	9.56	8.16	9.62	7.02	5.92	7.3
Na_2O	3.61	3.58	5.02	4.66	2.91	3.95	3.05	3.09	4.24	3.12	2.77	3.25	4.26	3.85
K_2O	0.95	0.83	1.96	1.28	1.10	1.22	1.5	2.12	0.5	0.67	0.59	1.07	1.04	1.05
TiO_2	0.62	0.61	0.54	0.69	0.47	0.58	1.07	1.06	1.17	1.04	1.15	1.09	0.85	1.01
P_2O_5	0.13	0.13	0.21	0.14	0.11	0.14	0.28	0.16	0.13	0.18	0.21	0.19	0.11	0.18
MnO	0.12	0.12	0.12	0.12	0.11	0.11	0.24	0.13	0.22	0.18	0.19	0.19	0.14	0.14
Cr_2O_3	0.009	0.009	0.002	0.002	0.007	0.005	0.031	0.036	0.021	0.022	0.021	0.026	0.017	0.02
LOI	5.3	4.9	2.4	4.1	4.2	4.18	3.9	3.8	6.9	4.7	4.9	4.84	4.88	4.06
Total	99.85	99.86	99.88	99.86	99.86	99.862	99.86	99.88	99.79	99.81	99.84	99.836	99.97	100.38
Ba	126	116	268	150	104	152.8	71	87	40	54	64	63.2	130.125	103.32
Co	13.7	13	4.6	12.7	10.6	10.92	17.5	14	10.3	17.2	14.9	14.78	25.81	23.2
Cs	0.4	0.2	0.1	0.2	0.2	0.22	0.9	0.8	0.1	0.4	0.4	0.52	0.36	0.16
Ga	14.2	13.9	14	14.2	14.5	14.16	14.8	16.7	15.2	14.3	16	15.4	17	14.62
Ni	77	81	94	68	20	68	185	134	70	95	57	108.2	87.09	88.36
Sc	19	19	11	19	17	17	42	41	36	30	33	36.4	33.55	28
Sr	197.2	180.1	171.3	189.7	183	184.26	191.7	170.7	145.2	274.3	390.9	234.56	340.62	193.2
Ta	0.2	0.2	0.1	0.2	0.2	0.18	0.1	0.1	0.1	0.1	0.1	0.1	0.24	0.18
Th	1.6	0.9	0.8	0.9	1.2	1.08	0.5	0.3	0.2	2.8	2.3	1.22	1.19	1.7
U	0.6	0.4	0.3	0.2	0.5	0.4	0.3	0.2	0.1	0.6	0.7	0.38	0.48	0.3
V	131	130	61	177	138	127.4	178	117	268	184	191	187.6	226.3	229
Zr	99.5	89.6	101.6	76.8	92.6	92.02	77.1	70.2	65.1	86	90.2	77.72	81.5	76.8
Y	27.1	25.2	26.3	21	25.3	24.98	29.8	24.4	26.9	26.2	29.9	27.44	22.5	28.8
Mo	0.1	0.2	0.1	0.1	0.2	0.14	0.2	0.2	0.2	0.2	0.2	0.2	…	0.86
Cu	25.1	22.9	3.1	26.1	18	19.04	32	10.4	4.4	67.2	71.2	37.04	60.3	36.78
Pb	1.1	1.6	0.2	0.4	0.6	0.78	1.5	1.4	1.3	2	2.5	1.74	2.87	0.8
Zn	72	72	64	61	59	65.6	74	62	100	69	63	73.6	54.3	54.3
As	0.5	0.5	0.5	0.5	0.5	0.5	9.2	4.1	5.1	2.8	4.3	5.1	…	1.37
Hf	2.8	2.4	2.9	2.1	2.6	2.56	2.1	1.8	1.7	2.6	2.5	2.14	2.07	2.4
Nb	2.4	2	2.1	1.7	2	2.04	1.2	0.9	0.5	1.9	2.4	1.38	3.87	1.6
Rb	14.6	10.6	16.9	14.8	17.5	14.88	27.7	40.1	8.6	12.6	12.2	20.24	13.18	28.8

Table 2b.

Elements (%)			Lake samples									
	P05	P025	P030	P035	P045	P055	P065	P075	P085	P095	P0105	P0115
SiO_2	45.6	46.14	46.45	46.33	47.86	50.86	47.05	49.54	48.24	47.71	53.06	44.69
Al_2O3	16.87	16.57	16.81	16.04	14.56	15.55	14.8	14.36	17.02	16.58	13.22	14.91
Fe_2O_3	9.48	9.42	9.61	9.41	8.29	8.45	8.71	7.89	8.6	8.83	7.29	8.9
MgO	5.48	5.51	5.58	5.51	5.36	4.95	5.54	5.23	5.35	5.62	4.62	5.79
CaO	5.18	5.2	4.83	5.92	7.8	5.71	7.24	7.15	4.61	4.79	9.14	8.01
Na_2O	1.3	1.34	1.36	1.63	1.97	2.1	1.86	1.73	1.16	1.18	1.81	1.77
K_2O	1.92	1.88	1.96	1.65	1.22	1.14	1.27	1.69	2.58	2.35	1.3	1.33
TiO_2	0.99	1.04	1.04	1.07	1.04	1.04	1.07	0.99	1.0	0.97	0.9	0.98
P_2O_5	0.18	0.18	0.18	0.17	0.16	0.14	0.15	0.17	0.17	0.16	0.14	0.17
MnO	0.19	0.18	0.19	0.18	0.17	0.14	0.17	0.15	0.14	0.17	0.15	0.18
Cr_2O_3	0.032	0.031	0.031	0.03	0.028	0.031	0.028	0.027	0.027	0.029	0.019	0.031
LOI	12.6	12.3	11.7	11.9	11.4	9.7	11.9	10.9	10.9	11.4	8.2	13.0
Total	99.81	99.81	99.81	99.82	99.83	99.85	99.82	99.82	99.8	99.8	99.83	99.82
Ba	311	319	344	291	225	159	240	295	417	391	260	220
Co	34.8	33.4	38.5	39	33	33	33.7	34.7	29.7	35.2	24.3	35.7
Cs	5.3	5.2	4.2	3.7	2.1	1.9	2.3	4	6.5	6.6	2.5	2.6
Ga	17.7	17.3	18.7	17.3	15.8	15.9	14.7	14.2	18.3	18.5	14	14.9
Ni	3.6	3.6	3	3.8	3.2	2.9	3.8	3.9	3.8	3.9	58.9	91.8
Sc	8.8	8.8	9	7.7	6.9	5.4	6.7	7.1	9.6	9.6	23	28
Sr	180.3	180.7	181.2	211.3	247.6	199.9	235.9	218.9	177.1	186.4	297	263.4
Th	5.6	5.6	6 .3	5.1	4.6	3.1	3.9	5.2	7.3	6.2	3.7	3.5
U	1.4	1.5	1.8	1.4	1.1	0.8	1.2	1.3	2	1.7	1.1	1.3
V	199	196	203	202	188	211	191	173	192	189	176	217
Zr	127.7	128.3	133.5	139.2	135.8	105.6	132.7	136.9	143.9	146.6	146.6	104.6
Y	23.6	25.8	27.9	28.3	28	28	27	27	24.1	28.6	28.6	25
Cu	77.4	72.3	74.8	67.2	49.6	50.7	58.8	51.4	63.1	64.6	29.1	54.6
Pb	27.1	23	24.6	19.2	12.9	11.8	16.3	21.2	23.4	16.3	12.3	15
Zn	103	99	98	86	68	72	77	82	91	91	59	74
As	17.9	18.8	17.5	17.4	18.7	18.1	18.1	18.2	18.2	18.2	20.7	12.9
Hf	3.6	3.6	3	3.8	3.2	2.9	3.8	3.9	3.8	3.9	3.1	3.2
Nb	8.8	8.8	9	7.7	6.9	5.4	6.7	7.1	9.6	9.6	4	6.1
Rb	56.7	54	58.1	48	35.2	30	39.4	49.6	76.4	68.1	37.1	37.8
Na_2O/TiO_2	1.31	1.29	1.31	1.52	1.89	2.02	1.74	1.75	1.16	1.22	2.01	1.81
Rb/Sr	0.31	0.3	0.32	0.23	0.14	0.15	0.17	0.23	0.43	0.37	0.12	0.14
Th/U	4	3.7	3.4	3.7	4.2	3.8	3.2	4	3.7	3.7	4	3.7
Th/Co	0.16	0.17	0.16	0.13	0.14	0.09	0.12	0.15	0.25	0.18	0.15	0.10
Ni/Co	3.76	3.83	3.3	3.13	2.82	2.82	3.12	2.56	3.7	3.47	2.55	2.97
Cu/Zn	0.75	0.73	0.76	0.78	0.73	0.7	0.76	0.63	0.69	0.71	0.49	0.74
V/Cr	0.91	0.93	0.96	0.99	0.99	1	1	0.94	1.05	0.96	1.36	1.03
$U_{(A)}$	−0.5	−0.4	−0.3	−0.3	−0.4	−0.2	−0.1	−0.4	−0.4	−0.4	−0.1	0.1
CIA	66.86	66.57	67.35	63.55	62.33	63.47	66.76	62.6	67.09	66.77	64.77	61.57
CIW	78.93	78.12	78.11	73.97	68.09	68.13	69.67	70.56	80.9	80.22	67.83	82.24
CIW/CIA	1.18	1.17	1.15	1.16	1.09	1.07	1.04	1.12	1.2	1.2	1.04	1.33
ICV	1.44	1.47	1.45	1.57	1.76	1.5	1.74	1.72	1.37	1.43	1.9	1.8
C-Value	0.7	0.7	0.72	0.66	0.52	0.63	0.57	0.51	0.64	0.65	0.44	0.55

Table 2b. (Continued).

Elements (%)	Lake samples										
	P0125	P0135	P0145	P0155	P0160	P0165	P0175	P195	Average	St. dev.	PAAS
SiO_2	45.3	46.37	45.63	44.21	45.89	45.46	44.62	45.64	46.83	2.21	62.4
Al_2O3	14.3	15.53	14.38	13.87	15.07	15.54	14.22	16.76	15.35	1.15	18.78
Fe_2O_3	8.09	8.72	8.03	7.7	8.23	8.8	7.93	9.19	8.58	0.65	7.18
MgO	5.46	5.49	5.3	5.3	5.48	5.48	5.22	5.63	5.4	0.26	2.19
CaO	8.8	7.25	8.86	10.14	7.86	6.97	9.42	5.53	7.02	1.72	1.29
Na_2O	1.81	1.81	1.96	1.85	1.77	1.63	1.78	1.38	1.66	0.28	1.19
K_2O	1.28	1.29	1.23	1.26	1.41	1.57	1.33	1.83	1.57	0.4	3.68
TiO_2	0.89	0.96	0.91	0.88	0.93	0.97	0.91	0.97	0.98	0.06	0.99
P_2O_5	0.14	0.14	0.13	0.14	0.14	0.14	0.13	0.15	0.15	0.02	0.16
MnO	0.17	0.19	0.18	0.17	0.17	0.18	0.17	0.2	0.17	0.02	0.11
Cr_2O_3	0.029	0.032	0.032	0.031	0.034	0.031	0.029	0.034	0.03	0	0.01
LOI	13.5	12	13.2	14.2	12.8	13	14	12.4	12.05	1.43	…
Total	99.83	99.84	99.8	99.79	99.8	99.79	99.8	99.77	99.81	0.02	…
Ba	211	221	188	215	218	246	220	289	264	6.19	650
Co	30.9	34.6	31	31.6	31.9	33.5	30.4	36.2	33.26	3.26	23
Cs	2.3	3	2.2	2.2	2.9	3.3	2.6	4.5	3.5	1.46	15
Ga	13.2	17	13.4	12.6	13.6	15.1	13.1	17.1	15.62	2	15
Ni	92.7	98.5	85.9	83.4	104.1	93.5	91.3	108.7	47.22	45.77	55
Sc	26	28	27	25	27	28	26	29	17.33	9.74	16
Sr	276.1	238.6	268.1	303.6	246.5	222.4	294.8	193.4	231.16	42.44	200
Th	3.4	4.1	3.3	3.7	3.8	4.5	3.8	4.8	4.58	1.16	14.6
U	1.2	1.4	1.3	1.2	1.1	1.3	1.1	1.6	1.34	0.28	3.1
V	180	193	183	172	176	190	173	192	189.8	12.7	150
Zr	114.4	105.8	110.6	98.2	102.2	108.3	113.6	105.5	122	16.59	210
Y	23.4	23.8	24.2	20.5	22.2	22.1	23.2	21.7	25.15	2.61	27
Cu	53.1	62.2	46.7	41.5	53.5	55.8	49.3	71.9	57.38	12.05	50
Pb	13.7	13.8	11.9	12.3	16.4	16.4	14.9	24.6	17.36	4.92	20
Zn	67	73	66	56	72	74	71	92	78.55	13.5	85
As	13.1	10.9	10.9	11.4	12.5	13.1	14.6	15.8	15.85	3.09	55
Hf	2.7	3	2.8	2.8	3.2	3.1	2.9	3.5	3.29	0.41	5
Nb	6	6.4	8.2	7.9	7.8	7.8	7	8.4	7.46	1.44	1.9
Rb	34.1	35.9	29.5	31.7	36.1	41.5	33.5	51.4	44.21	13.13	160
Na_2O/TiO_2	2.03	1.89	2.15	2.1	1.9	1.68	1.96	1.42	1.7	0.22	1.2
Rb/Sr	0.12	0.15	0.11	0.1	0.15	0.19	0.11	0.27	0.2	0.05	0.8
Th/U	4	3.7	3.5	3.6	4.2	3.9	3.3	4	3.7	3.6	4.7
Ni/Co	2.55	2.97	3.3	3.27	3.52	3.92	4.23	3.97	3.28	3.98	2.39
Cu/Zn	0.49	0.74	0.79	0.85	0.71	0.74	0.74	0.75	0.71	0.78	0.58
V/Cr	0.91	0.89	0.84	0.82	0.76	0.99	0.88	0.83	0.95	0.12	1.36
U (A)	–0.1	0.1	0.1	0.1	0.2	0.1	–0.2	–0.2	–0.16	0.1	…
CIA	64.77	64.44	67.85	63.83	62.7	62.51	65.54	62.51	65.69	1.98	…
CIW	69.52	71.24	67.93	68.4	68.4	71.08	73.36	69.76	77.82	4.88	…
CIW/CIA	1.07	1.1	1	1.07	1.13	1.17	1.06	1.24	1.12	0.07	…
ICV	1.9	1.8	1.84	1.64	1.83	1.96	1.7	1.64	1.867	1.46	…
C-value	0.48	0.57	0.48	0.43	0.51	0.58	0.59	0.66	0.58	0.07	…

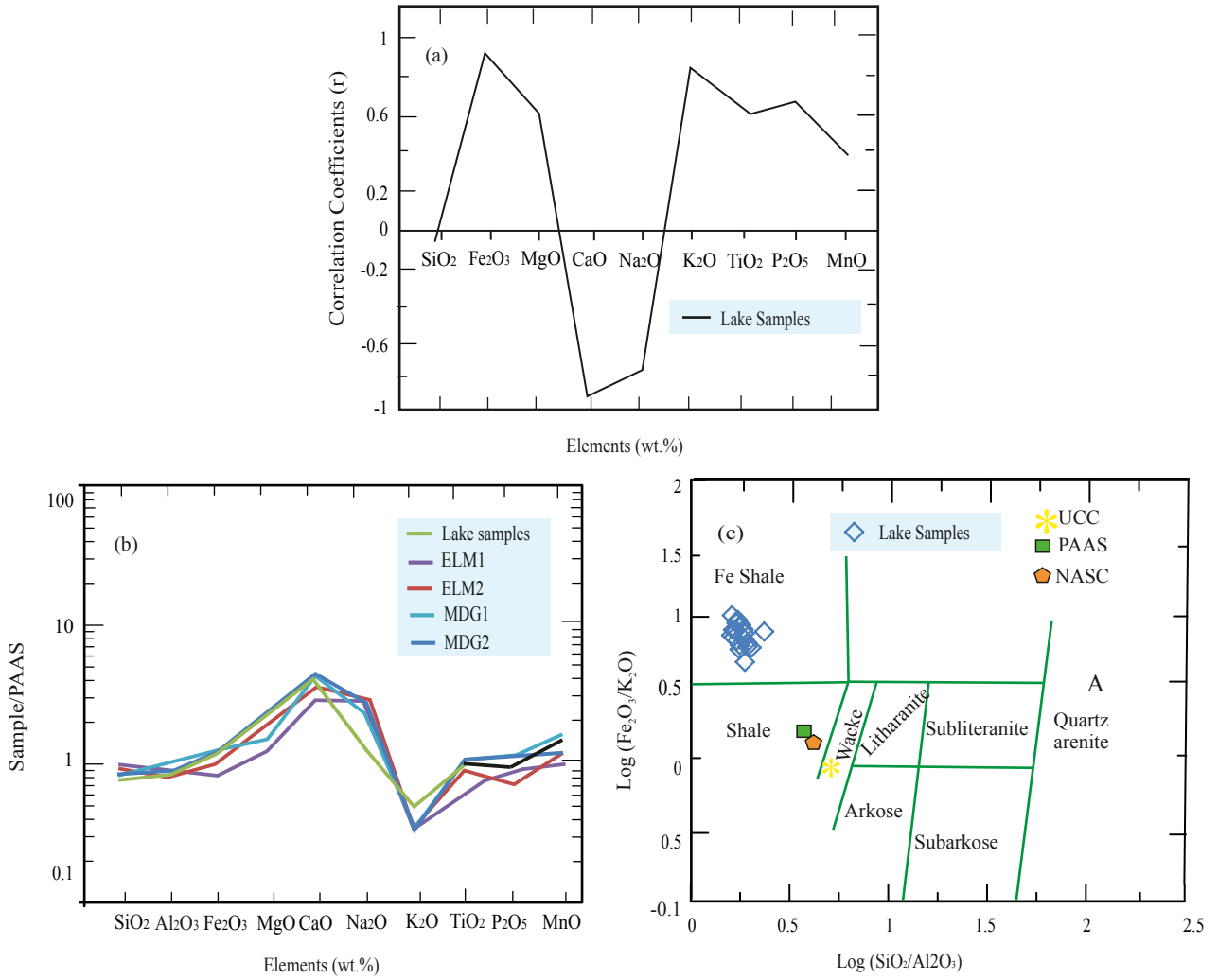

Figure 6. (a) Pearson correlation coefficients of major oxide elements with Al_2O_3 for lake samples. (b) Major element enrichment relative to PAAS for lake samples, surrounding rocks, Elazığ magmatics (ELM1: this study), Maden Group (MDG1: this study), ELM2 (from Dönmez, 2006, n = 15), MDG2 (from Ertürk et al., 2018, n = 8) (PAAS composition from Taylor and McLennan, 1985). (c) Scattering of log (Fe_2O_3/K_2O) vs. log (SiO_2/Al_2O_3) from Herron (1988) for lake samples. UCC: Upper continental crust (McLennan, 2001); PAAS: Post-Archean Australian shales (Taylor and McLennan, 1985); NASC: North American shale composite (Gromet et al., 1984).

values of Taylor and McLennan (1985) are included as a reference. As shown in Figure 7a, Th, Ga, Cs, Pb, and Zn, which are positively correlated with Al_2O_3, also have high positive correlations with total REEs, indicating that REEs are associated with clay minerals (Figure 8). REEs are absorbed by clay minerals (Milodowsky and Zalasiewicz, 1991; Coppin et al., 2002). Cu, Pb, and Zn are chalcophile elements that are bounded to sulfide minerals (Kiseeva et al., 2017). However, the positive correlation of these elements with ΣREEs might be due to their strong association with clays rather than sulfides (Figure 8).

Chondrite-normalized REE patterns of lake samples ELM and MDG were compared with the PAAS normalized patterns (Taylor and McLennan, 1985). The average chondrite normalized REE patterns of the lake samples and surrounding rocks ELM1–2 and MDG1–2 are different from the PAAS (Tables 3a and 3b; Figure 9). These patterns show that lake samples are enriched in light rare earth elements (LREEs) [average $(La/Sm)_{CN}$ is 2.76], have relatively flat heavy rare earth elements (HREEs) [average $(Gd/Yb)_{CN}$ is 1.38], and have a low negative Eu anomaly (average Eu/Eu* = 0.90) (Table 3b). The chondrite-normalized Elazığ magmatics show slightly enriched LREEs with $(La/Sm)_N$ = ELM1: 1.67 and ELM2: 1.32 and HREEs with $(Gd/Yb)_N$ = ELM1: 1.11 and ELM2: 1.37 patterns, and a low negative Eu anomaly of Eu/Eu* (ELM1: 0.93–ELM2: 0.64). The Maden Group shows slight enrichment of LREEs with $(La/Sm)_N$ = MDG1: 1.83 and

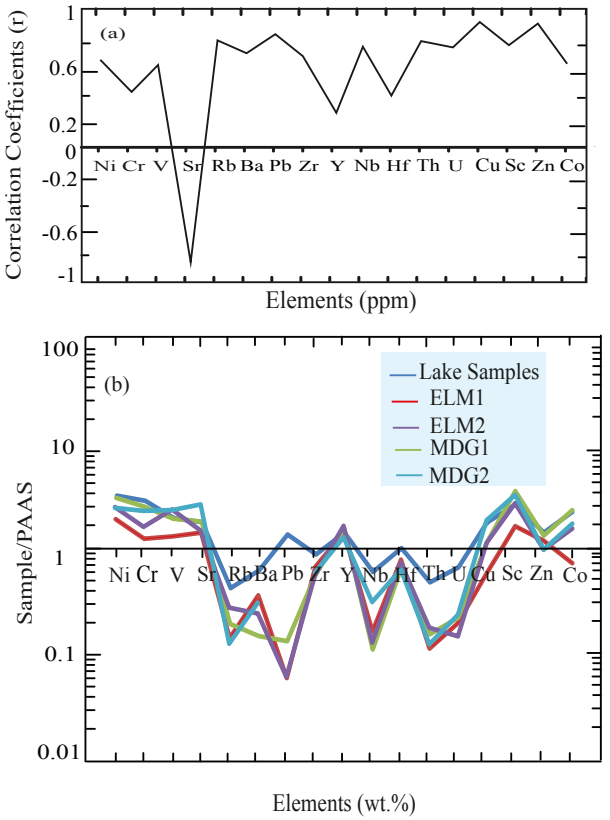

Figure 7. (a) Pearson correlation coefficients of selected trace elements with Al_2O_3 for lake samples. (b) Average of trace element enrichment plot (relative to PAAS) for lake samples, surrounding rocks (ELM1-2), Maden Group (MDG1-2) (PAAS composition from Taylor and McLennan, 1985).

MDG2: 1.87 and flat HREEs with $(Gd/Yb)_N$ = MDG1: 1.25 and MDG2: 1.14 patterns with Eu/Eu* = MDG1: 0.82 and MDG2: 0.94 (Table 3b). The average chondrite-normalized REE patterns of lake sediments are similar to those of bedrock. The average shales have a Ce/Ce* value of 1.0 (Cullers and Berendsen, 1998). The average Ce/Ce* value of lake samples is 0.94, which is consistent with average shale values (Table 3b). This is also supported by the geochemical classification diagram in Figure 6c.

5. Discussion

5.1. Source rock weathering

The chemical index of alteration (CIA) is widely used to find out the degree of chemical weathering. The intensity is calculated with the chemical index of alteration: CIA = $[Al_2O_3 / (Al_2O_3 + Na_2O + K_2O + CaO^*) \times 100]$, where CaO* is the CaO associated with the silicate fraction (Nesbitt and Young, 1982). Total CO_2 content was not determined. Therefore, we cannot introduce correction for the carbonates to obtain true CaO*. In this study, CaO was initially corrected for phosphate using available P_2O_5 data (CaO* mol CaO mol $P_2O_5 \times 10 / 3$) (Maynard, 1992; Fedo et al., 1995). If the remaining mole number is less than that of Na_2O, then the CaO value is accepted as the CaO*. Otherwise, the CaO* is assumed to be equivalent to Na_2O (McLennan, 1993; Bock et al., 1998; Vital and Stattegger, 2000; Roddaz et al., 2006; Mourabet et al., 2018). Following the phosphate correction, CaO values are found to be higher than Na_2O. Thus, the molar proportion of Na_2O is used as the molar proportion of CaO according to the indirect method of McLennan et al. (1993). In this index, the CIA values of the igneous rocks and feldspars are around 50, and shales have values of about 70–75; on the other hand, in residual clays it may reach almost 100 (Nesbitt and Young, 1982; Fedo et al., 1995) (Figure 10a; Table 2b). The CIA provides semiquantitative information on the paleoclimate of the source rock. Low CIA values (50 or less) might also reflect cool and/or arid conditions without abundant rainfall (Fedo et al., 1995; Tang et al., 2012). For humid climates, CIA values of >80 indicate high-degree alteration of source rocks (Mourabet et al., 2018). CIA values of lake samples varying from 61.57 to 67.85 (average: 65.98) show a low to moderate degree of alteration of the source rocks and indicate that humid conditions did not reign. This was also reflected in the type of clay minerals. A clay mineral assemblage dominated by chlorite and illite is typical of soils and sediments produced in high latitudes or by cold-climate weathering because chemical weathering in such settings is weak (Bockheim et al., 1998). Chlorite does not generally survive under cool, moist temperature and its presence in sediments as a detrital clay is a good indicator of cool/dry climates (Chamley, 1989), whereas smectites and smectite/chlorite mixed-layer clays are products of warm and wet climate conditions (Chamley, 1989). Hseu et al. (2007) stated that under more humid conditions, concentrations of Fe, Mg, and hydroxyl ions within chlorite decrease and as a result chlorite is transformed into an expanding clay mineral such as smectite. The presence of chlorite in studied samples is consistent with a cold-climate regime and the existence of S-C is indicative of very humid conditions. The coexistence of both minerals reflects a semidry and semihumid climate. No kaolinite was recorded. Kaolinite is formed during advanced stages of chemical weathering (Liu et al., 2005). Lack of kaolinite in core sediments can be interpreted as a sign of low to moderate alteration in the lake sediments. It is predicted that the weathering did not advance up to the formation of kaolinite even under wet climates.

Weathering effects can also be evaluated with the formula of chemical index of weathering (CIW) = $Al_2O_3 / (Al_2O_3 + CaO^* + Na_2O) \times 100$ (Harnois, 1988). This index is more suitable for the carbonate-bearing siliciclastic rocks.

Table 3. REE concentrations and some elemental ratios of (a) surrounding rocks, Elazığ magmatics (ELM1: this study), Maden Group (MDG1: this study), ELM2 (from Dönmez, 2006, n = 15), MDG2 (from Ertürk et al., 2018, n = 8). (b) Lake samples. The cerium anomaly (Ce/Ce*) was estimated by the equation $Ce/Ce^* = 2Ce_N / (La_N + Pr_N)$, $Eu / Eu^* = Eu_N / (Sm_N \cdot \times Gd_N)^{1/2}$, where subscript $_N$ indicates the normalized abundance with chondrites after Taylor and McLennan (1985), same as in $(La/Lu)_N$, $(La/Yb)_N$, $(La/Sm)_N$, $(Gd/Yb)_N$.

Table 3a.

							Surrounding rocks								
Elements (ppm)	ELM1							MDG1							
	Sample no.	HE1	HE2	HE3	HE4	HE5	Average	HM1	HM2	HM3	HM4	HM5	Average	ELM2	MDG2
La	9.1	8	8.5	6.7	7.4	7.9	7.93	5	2.9	12.8	12.1	8.1	8.18	38	9.29
Ce	20.2	17.2	19.8	14.5	17.3	17.8	17.80	10.2	6.8	23.8	22.2	15	15.6	80	20.99
Pr	3.06	2.65	3.07	2.37	2.66	2.8	2.77	1.86	1.41	3.33	3.29	2.5	2.47	8.83	2.86
Nd	13.8	13	14.6	10.5	12.3	12.8	12.83	9.3	7.4	15.2	15.1	11.9	11.7	33.9	12.98
Sm	3.37	3.16	3.44	2.62	3.0	3.1	3.12	2.77	2.78	3.5	3.69	3.2	3.18	5.6	3.23
Eu	1.04	1.01	1.11	0.93	1.06	1.0	1.03	0.93	1.0	1.14	1.34	1.1	1.10	1.1	1.08
Gd	3.88	3.72	3.89	3.12	3.7	3.7	3.67	3.6	3.92	4.37	4.43	4.2	4.10	4.66	3.62
Tb	0.7	0.65	0.71	0.55	0.67	0.7	0.66	0.66	0.69	0.73	0.8	0.7	0.71	0.77	0.6
Dy	4.5	4.17	4.33	3.47	4.05	4.1	4.10	4.05	4.43	4.39	4.91	4.5	4.45	4.68	3.79
Ho	1.02	0.9	0.93	0.79	0.98	0.9	0.92	0.93	1.05	0.96	1.18	1.0	1.02	0.99	0.79
Er	2.98	2.57	2.77	2.3	2.8	2.7	2.69	2.71	2.84	2.72	3.5	3.0	2.95	2.85	2.31
Tm	0.45	0.41	0.44	0.37	0.44	0.4	0.42	0.38	0.42	0.42	0.52	0.4	0.42	0.4	0.35
Yb	3.1	2.84	2.89	2.32	2.88	2.8	2.81	2.5	2.74	2.67	3.27	2.8	2.79	2.8	2.25
Lu	0.52	0.43	0.48	0.39	0.46	0.5	0.46	0.39	0.44	0.44	0.53	0.5	0.46	0.43	0.34
∑REE	67.7	60.7	66.96	50.9	59.7	61.2	61.19	45.3	38.8	76.5	76.9	59.1	59.3	185	50.4
Ce/Ce*	0.93	0.91	0.94	0.89	0.95	0.9	0.92	0.81	0.82	0.87	0.84	0.8	0.82	0.84	0.80
Eu/Eu*	0.93	0.94	0.92	0.95	0.96	0.9	0.93	0.99	1.03	0.97	0.95	0.99	0.98	0.64	0.94
$(La/Lu)_N$	1.93	2.05	1.96	1.9	1.78	1.9	1.92	1.42	0.73	3.21	2.52	2.4	2.05	7.68	2.37
$(La/Yb)_N$	2.17	2.08	2.17	2.13	1.9	2.1	2.09	1.48	0.78	3.54	2.74	1.3	1.96	10.03	3.06
$(La/Sm)_N$	1.76	1.65	1.61	1.67	1.61	1.7	1.67	1.18	1.68	2.39	2.14	1.8	1.83	1.32	1.87
$(Gd/Yb)_N$	1.06	1.11	1.14	1.14	1.09	1.1	1.11	1.22	1.21	1.39	1.15	1.3	1.25	1.37	1.14

Table 3b.

Elements (ppm)				Lake samples									
	P05	P025	P030	P035	P045	P055	P065	P075	P085	P095	P0105	P0115	P0125
La	19.8	20.1	20.9	18.4	16.9	17.2	19	25.2	23.1	23.1	14.7	14.4	14.2
Ce	40.9	41.8	44.5	36.6	32.8	32.5	35.4	38.6	47.2	50.2	30.3	29.5	27.3
Pr	4.73	4.97	4.98	4.66	4.27	4.04	4.77	5.7	5.7	5.7	3.84	3.66	3.79
Nd	20.4	19.1	19.9	18.5	18.3	17.7	20.7	20.9	24.4	24.4	15.9	16.1	16.7
Sm	4.33	4.38	4.48	4.51	4.4	4.2	4.35	4.81	4.95	4.95	3.91	3.84	3.62
Eu	1.04	1.16	1.2	1.26	1.26	1.17	1.19	1.17	1.28	1.28	1.31	1.09	1.07
Gd	4.67	4.77	4.99	4.81	4.58	4.62	4.77	4.92	4.94	4.94	4.75	4.21	3.92
Tb	0.78	0.8	0.81	0.8	0.82	0.81	0.74	0.82	0.82	0.82	0.76	0.74	0.63
Dy	4.36	4.91	4.73	4.77	4.74	5.16	4.92	4.32	5.18	5.18	4.56	4.21	3.59

Table 3b. (Continued).

Ho	0.96	1.06	1.07	1.1	1.1	0.93	0.89	0.92	0.93	0.93	0.88	0.9	0.75
Er	2.54	3.24	3.16	3.09	3.47	2.94	2.62	3.1	2.95	2.95	2.78	2.85	2.5
Tm	0.42	0.45	0.46	0.48	0.41	0.4	0.41	0.44	0.41	0.41	0.37	0.38	0.38
Yb	2.93	2.91	3.11	3.08	3.1	2.95	2.4	2.88	2.94	2.94	2.5	2.47	2.57
Lu	0.4	0.43	0.51	0.49	0.47	0.42	0.39	0.41	0.43	0.43	0.38	0.36	0.32
ΣREE	108.3	110.1	114.8	102.6	96.6	89.5	97.9	105.8	122.8	128.2	86.9	84.7	81.3
Ce/Ce*	1..01	0.99	1.03	0.93	0.91	1.02	1.01	0.96	0.93	1.03	0.95	0.96	0.88
Eu/Eu*	0.9	0.9	0.9	0.89	0.87	0.91	0.91	0.88	0.87	0.95	0.91	0.90	0.97
$(La/Lu)_N$	5.47	5.16	4.53	4.15	3.66	4.52	5.38	6.79	5.93	4.27	4.42	4.90	4.09
$(La/Yb)_N$	4.99	5.11	4.97	4.42	3.94	4.31	5.85	6.47	5.81	4.35	4.31	4.08	4.32
$(La/Sm)_N$	2.98	2.99	3.04	2.66	2.5	2.12	2.67	2.85	3.42	3.04	2.45	2.45	2.56
$(Gd/Yb)_N$	1.35	1.39	1.36	1.33	1.26	1.42	1.33	1.26	1.42	1.43	1.62	1.45	1.30

Table 3b. (Continued).

Elements (ppm)	Lake samples								
	P0135	P0145	P0155	P0160	P0165	P0175	P0195	Average	PAAS
La	15.2	14.6	14.1	15.3	15.3	16.9	14.4	17.64	38.0
Ce	28.8	26.1	27.2	28.8	32.2	27.6	35.2	34.68	80.0
Pr	3.68	3.36	3.44	3.74	3.74	3.99	3.63	4.32	8.8
Nd	14.9	14.4	14.2	15.2	15.2	16.5	14.8	17.91	33.9
Sm	3.48	3.2	3.44	3.76	3.9	3.76	4.11	4.12	5.6
Eu	1.03	0.9	0.98	1.01	1.08	0.98	1.03	1.12	1.1
Gd	4.4	3.57	3.63	3.85	4.1	3.77	4.3	4.43	4.7
Tb	0.75	0.62	0.62	0.65	0.7	0.64	0.75	0.74	0.8
Dy	4.2	3.84	3.85	3.86	4.34	3.79	4.5	4.45	4.7
Ho	0.96	0.79	0.8	0.81	0.91	0.82	0.96	0.92	1.0
Er	2.74	2.45	2.32	2.31	2.65	2.59	2.82	2.8	2.9
Tm	0.42	0.32	0.37	0.36	0.39	0.36	0.4	0.4	0.4
Yb	2.6	2.28	2.23	2.37	2.42	2.28	2.66	2.68	2.8
Lu	0.41	0.34	0.35	0.36	0.4	0.37	0.42	0.4	0.4
ΣREE	83.6	76.8	77.5	82.4	90.5	79.8	99.7	95.99	185
Ce/Ce*	0.92	0.91	0.88	0.92	0.9	0.92	0.9	0.94	-0.01
Eu/Eu*	0.91	0.89	0.88	0.89	0.87	0.89	0.89	0.9	0.64
$(La/Lu)_N$	4.74	4.45	4.69	4.67	4.3	5.1	5.1	4.82	7.68
$(La/Yb)_N$	4.73	4.67	4.77	5.16	4.67	5.39	5.39	4.89	10.03
$(La/Sm)_N$	2.85	2.98	2.67	2.65	2.83	2.5	3.08	2.76	4.42
$(Gd/Yb)_N$	1.44	1.33	1.38	1.38	1.44	1.41	1.37	1.38	1.37

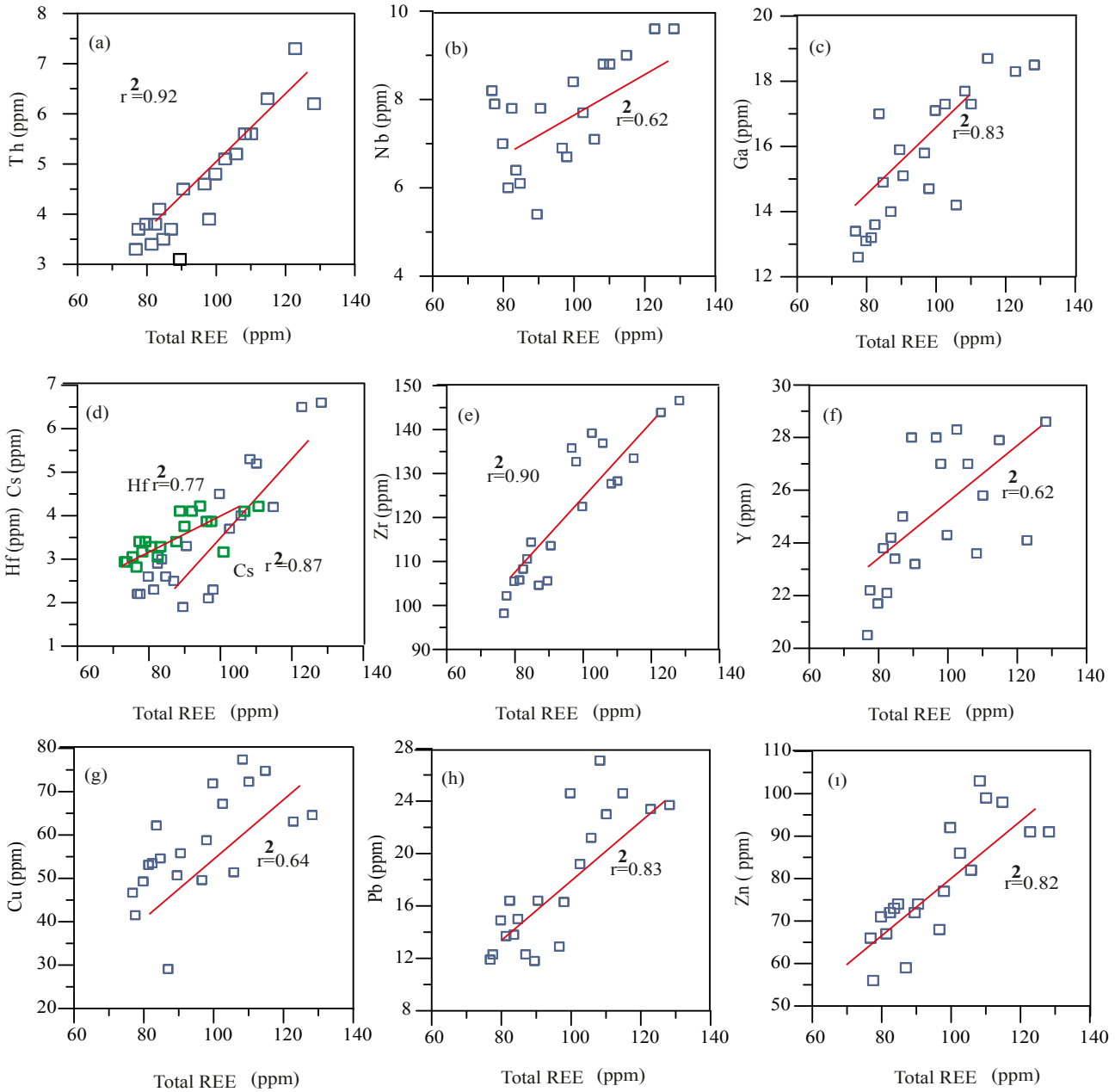

Figure 8. Correlation graphics between selected trace elements and total REEs.

This equation is more appropriate for understanding the extent of plagioclase alteration alone (Malick and Ishiga, 2016). CIW is interpreted in a similar way with a CIA value of 50 for unweathered upper continental crust and about 100 for highly weathered materials with complete removal of alkali and alkaline-earth elements (McLennan, 1993; Mongelli et al., 1996). A low CIW/CIA ratio is characteristic of immature crustal material from local sources. This material has experienced a short distance of transport until final deposition (Gao and Wedepohl, 1995; Eker, 2012). CIW/CIA values are low in the lake samples, showing that the studied sediments are transported to the lake basin from the surrounding rocks nearby (Table 2b; averages: 1.11%). This is also supported by the evidence of clay morphology. In SEM examinations, the shape of clays displayed thicker plates and rounded outlines. Such textures of clays point to physical weathering triggered by rapid erosion (Song et al., 2014).

Na can be easily removed during chemical weathering. The Na_2O/TiO_2 ratio may also be reduced by chemical weathering (Ling et al., 2013). Na_2O/TiO_2 ratios are negatively correlated with CIA in lake samples (r = –0.69)

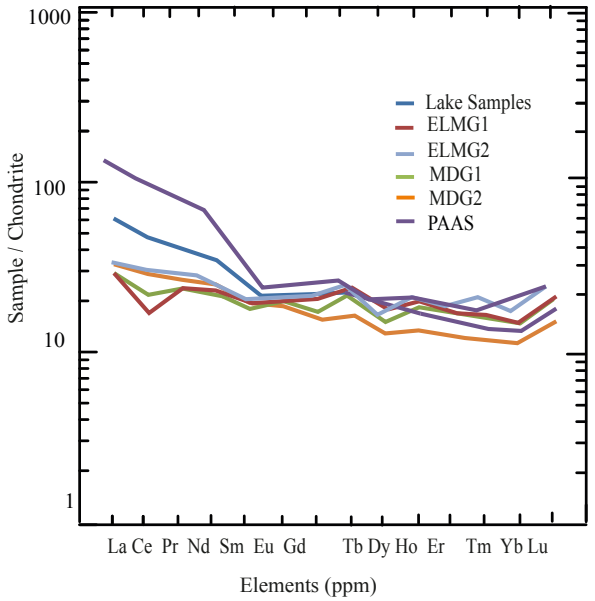

Figure 9. Comparison of chondrite-normalized average values of the lake samples, surrounding rocks, Elazığ magmatics (ELM1: this study), Maden Group (MDG1: this study), ELM2 (from Dönmez, 2006, n = 15), MDG2 (from Ertürk et al., 2018, n = 8), and PAAS composition from Taylor and McLennan, 1985). Normalizing values are from Taylor and McLennan (1985).

(Figure 10b). Sr has a stronger chemical mobility relative to Rb during alteration, and this gives rise to an increase in Rb/Sr ratio and alteration degree (Nesbitt and Young, 1982). Rb/Sr is positively correlated with CIA in lake samples (r = 0.65), which might be related to weathering (Figure 10c).

The LREE pattern of lake samples is enriched with respect to the bedrock of Elazığ magmatics and the Maden Group (Figure 9). This LREE enrichment in the lake samples is probably related to the low to moderate degree of chemical weathering of the source rocks because HREEs are preferentially mobilized during weathering (Sholkovitz, 1988). This explains the high value of $(La/Sm)_{CN}$ with respect to source rock (Tables 3a and 3b). In fact, $(La/Sm)_{CN}$ shows a positive correlation with CIA in lake samples (r = 0.50) (Figure 10d).

Index of compositional variability (ICV) = $(Fe_2O_3 + K_2O + Na_2O + CaO + MgO + TiO_2) / Al_2O_3$) is used to calculate the quantity of primary source relative to weathered minerals (Cox et al., 1995; Hernández-Hinojosa et al., 2018). Immature shales with a high percentage of nonclay silicate minerals have values >1, whereas mature sediments have values of <1 (Johnsson, 2000; Cullers, 2002). These values of the lake samples vary between 1.37 and 1.96, characteristic of immature material from local sources (Table 2b). This may indicate that coarse clastics are derived from nearby source rocks and these clastics are slightly dissolved, since limited transportation took place until final deposition (Toulkeridis et al., 1999; Eker and Korkmaz, 2011; Mourabet et al., 2018).

Zhao et al. (2007) used the ratio of ∑ (Fe + Mn + Cr + Ni + V + Co) / ∑ (Ca + Mg + Sr + Ba + K + Na) (C-value) to study the paleoclimate of China's Junggar Basin and suggested that this ratio is between 0.2 and 0.8 for semiarid to semihumid climates. The C-values of Lake Hazar samples range between 0.44 and 0.72, which mainly shows semiarid to semimoist climatic conditions over the last 2000 years (Figure 10; Table 2b). Considering the variations in C-value, lower levels of the studied piston are represented by semiarid to semihumid climate conditions, whereas upper parts with increasing C-values correspond to a semihumid regime. This is also supported by Ca/Ti ratios that increase with increasing C-values (Figure 11). Ca is most likely derived from endogenic calcite; Ti is an immobile element related to detritic input. In areas where Ca/Ti ratios are decreased, the detrital contribution increases (Fischer and Wefer, 1999). These findings are consistent with the results of Biltekin et al. (2018), who proposed arid to cold climate conditions during the late Holocene (1.4 ka BP) on the basis of pollen records. Eriş et al. (2018b) documented a similar result based on the μ-XRF Ca/Ti and Sr/Ca data from the sediment core, implying a rising lake level due to wetter climate conditions during the last 1.4 ka. According to Eriş (2013), the youngest transgressive deltaic deposition took place at the mouth of the Kürkçayı River during the same time interval, attesting to a progressive rise in the lake level.

5.2. Redox conditions

U, Th, V, Cr, Ni, Co, Cu, and Zn elements are redox-sensitive and provide reconstructions of oxygen conditions in sedimentary environments (Martinez-Ruiz et al., 2015). Geochemical parameters such as authigenic U, Th/U, Ni/Co, V/Cr, and Cu/Zn are very helpful for determining paleoredox conditions during sediment deposition (Wignall and Myers, 1988; Tribovillard et al., 2006; Yang et al., 2011; Rimmer, 2004; Mir, 2015). The authigenic uranium content (U_A) is regarded as an index of bottom water condition and is calculated as authigenic U = (total U) – Th / 3. An authigenic U concentration below 2 suggests oxic conditions of deposition, whereas values above 2 indicate dysoxic conditions (Wignall and Twitchett, 1996). Similarly, the Th/U ratio is utilized for redox conditions of the depositional environment (Kimura and Watanabe, 2001). These ratios vary from 0 to 2 in anoxic environments and from 2 to 7 in oxic environments (Wignall and Twitchett, 1996; Hara et al., 2010). In the lake sediments, authigenic uranium content is low (changing from –0.5 to 0.1) and $(U)_A$ contents are less than one; Th/U ratios vary between 3.2 and 4.2, displaying an oxygen-enriched depositional environment (Table 2b).

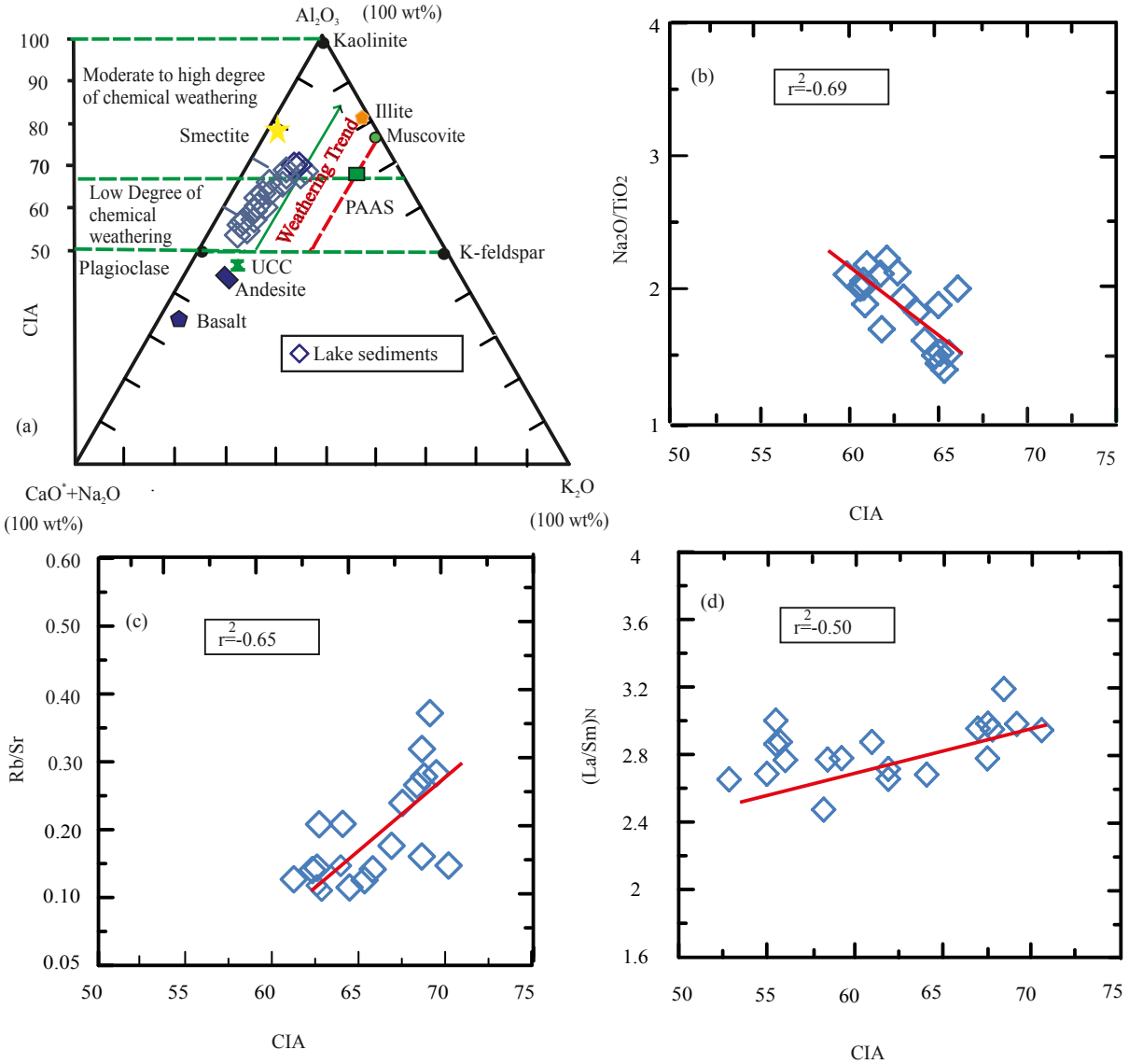

Figure 10. (a) A-CN-K ternary diagram of Al_2O_3 – (Ca + Na_2O) – K_2O for the lake samples (after Nesbit and Young, 1982). UCC average (upper continental crust) and PAAS (Post-Archean Australian shale) from Taylor and McLennan (1985). Correlation coefficients between CIA indices and (b) Na_2O/TiO_2 and (c) Rb/Sr (d) $(La/Sm)_N$ elemental ratios.

The Ni/Co ratio is also used as a redox indicator (Dypvik, 1984). It is proposed that Ni/Co ratios of <5 indicate oxic environments, while a ratio of >5 proposes suboxic and anoxic environments (Jones and Manning, 1994). The V/Cr ratio is another sensitive indicator for determination of paleoredox conditions. High V/Cr values are accepted as an indicator of anoxic conditions (Dill, 1986; Jones and Manning, 1994). While high Cu/Zn ratios show reducing depositional conditions, low ratios propose oxidizing conditions (Hallberg, 1976; Nagarajan et al., 2007). Ni/Co and V/Cr ratios of the studied samples suggest oxic conditions for the lake environment (Figure 12). Lake Hazar sediments have Cu/Zn ratios between 0.49 and 0.85, indicating oxic conditions for the depositional environment (Table 2b).

Eu and Ce anomalies in REE patterns are generally used to expose the redox conditions (Guo et al., 2007). Average Eu/Eu* and Ce/Ce* values of the lake sediments are 0.90–0.94, respectively, showing an enhanced Eu and Ce abundance in an oxic depositional environment (Shields and Stille, 2001) (Table 3b). Similarly, Möller and Bau (1993) studied the aerobic alkaline (pH 9.6) waters of Lake Van in Eastern Turkey and reported positive Ce anomalies in REE patterns of alkaline aerobic lake waters. Lack of Ce anomaly in lake waters also results from the alkaline character of Lake Hazar in the last 2000 years (Figure 9).

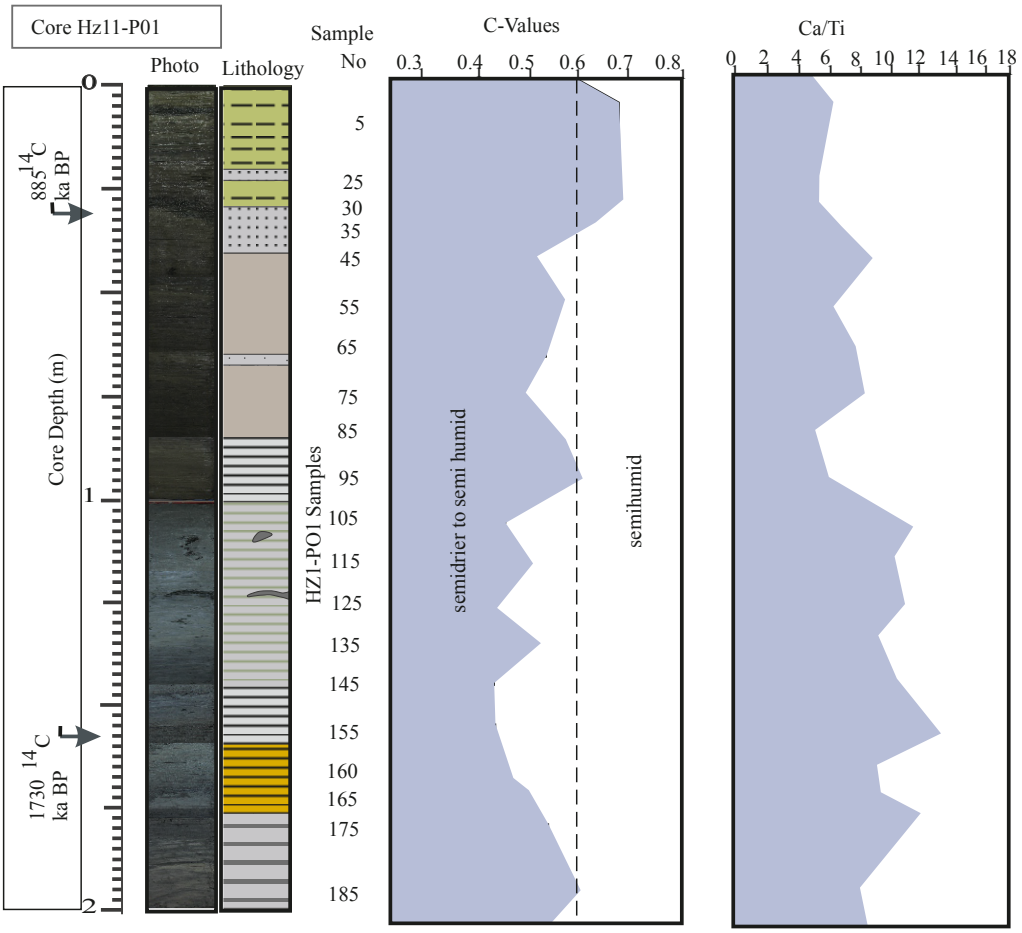

Figure 11. C-value = [Σ (Fe + Mn + Cr + Ni + V + Co) / Σ (Ca + Mg + Sr + Ba + K + Na)] (Zhao et al., 2007) and Ca/Ti ratios of lake samples, reflecting paleoclimatic conditions.

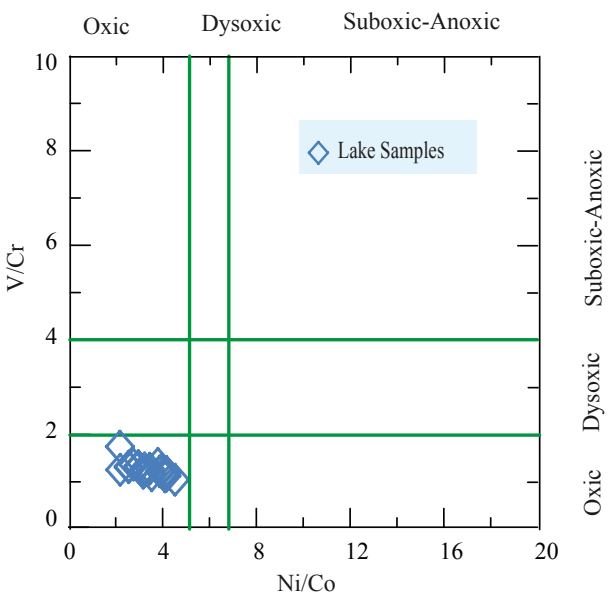

Figure 12. Ni/Co vs. V/Cr plot of lake samples (after Rimmer, 2004).

5.3. Provenance

Several investigations have demonstrated that the chemical compositions of siliciclastic sedimentary rocks are related to those of their source rocks (Cullers, 1995; McLennan, 2001; Armstrong-Altrin et al., 2004, 2012, 2013). Several major-, trace-, and REE-based discrimination diagrams have been proposed by various authors (e.g., Roser and Korsch, 1986; Floyd et al., 1989; McLennan at al., 1993). On the major element-based provenance discriminant function diagram of Roser and Korsch (1986), lake samples fall into the mafic (three samples in intermediate) igneous provenance (Figure 13a).

Ratios of some elements are used for discriminating felsic from mafic source components in sedimentary rocks (Taylor and McLennan, 1985). Felsic rocks have higher La, Zr, and Th amounts than mafic rocks, while the amounts of Co, Sc, and Cr are higher in mafic rocks (Mishra and Sen, 2012). La/Sc, Th/Sc, Th/Co, and Cr/Th ratios have been used to differentiate sediments derived from different source rocks (Cullers et al., 1988; Cullers and Podkovyrov,

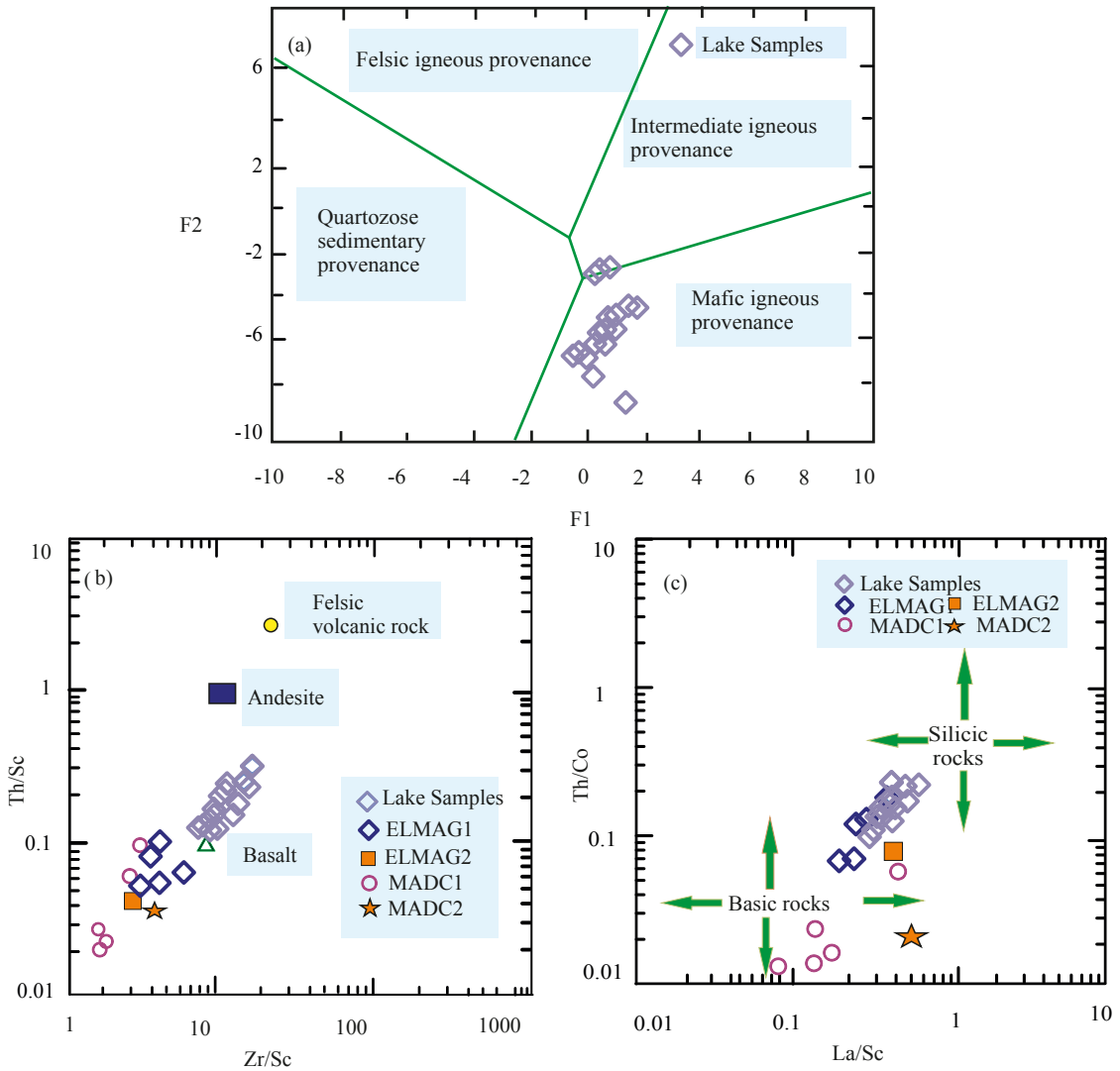

Figure 13. (a) Discriminant function diagram of lake samples showing the provenance (Roser and Korsch, 1986). The discriminant functions are as follows: discriminant function F1 = (–1.773 × TiO_2) + (0.607 × Al_2O_3) + (0.760 × Fe_2O_3) + (–1.500 × MgO) + (0.616 × CaO) + (0.509 × Na_2O) + (–1.224 × K_2O) + (–9.090); discriminant function 2 = (0.445 × TiO_2) + (0.070 × Al_2O_3) + (–0.250 × Fe_2O_3) + (–1.142 × MgO) + (0.438 × CaO) + (1.475 × Na_2O) + (1.426 × K_2O) + (–6.861). (b) Zr/Sc vs. Th/Sc plot after McLennan et al. (1993). (c) La/Sc vs. Th/Co diagram (fields after Cullers, 2002) for lake samples, surrounding rocks, Elazığ magmatics (ELM1: this study), Maden Group (MDG1: this study), ELM2 (from Dönmez, 2006, n = 15), MDG2 (from Ertürk et al., 2018, n = 8).

Table 4. Range of elemental ratios in lake samples compared to ratios in similar fractions derived from mafic rocks (Cullers, 2002). Sediments derived from mafic rocks, sediments from felsic rocks from Cullers (1994).

Elemental ratio	Average of lake samples	Range of sediments		PAAS
		Mafic rocks	Felsic rocks	
La/Sc	0.64	0.4–1.1	1.6–2.5	2.40
Th/Sc	0.16	0.04–0.05	0.83–20	0.90
Co/Th	7.69	7.1–8.3	0.22–1.5	1.57
Cr/Th	46.87	22–100	0.5–7.7	7.53

2000). La/Sc and Cr/Th element ratios in lake samples are representative of sediments derived from mainly mafic source rocks (Table 4). Th/Sc ratios are between the values of sediments derived from mafic source rocks and felsic rocks. The diagrams based on Zr/Sc vs. Th/Sc and La/Sc vs. Th/Co ratios also show that the composition of source rocks varies from mafic to felsic but is mostly dominated by a mafic contribution (Figures 13b and 13c).

REEs have also been utilized to show the chemical composition of the source rocks since felsic rocks contain high LREE/HREE ratios and negative Eu anomalies, whereas mafic rocks have low LREE/HREE ratios and no Eu anomalies (Cullers and Graf, 1983). The absence of distinct Eu anomalies indicates that they originated from undifferentiated to slightly differentiated mafic (basalt-andesite) units (McLennan et al., 1993) (Table 2b; Figure 9). Lower LREE abundances with respect to PAAS also reflect the mafic nature of Lake Hazar sediments (Figure 9). This finding is consistent with the results of previous studies. According to Aksoy et al. (2007), Eriş et al. (2013), and Eriş et al. (2018b), Lake Hazar deposits are contributed by the Kürkçayı River and alluvial fans and the Elazığ magmatics and Maden Group rocks at the western part of the lake. These rocks are mostly of mafic composition (Ural et al., 2015; Ertürk et al., 2018), which is also reflected in clay mineralogy. Chlorite is formed by the weathering of intermediate and basic crystalline rocks with degradation of preexisting ferromagnesian minerals (Millot, 1970). Alt et al. (1986) found phyllosilicates, such as chlorites, within low-degree metamorphosed metabasites. Yang et al. (2016) mentioned illite occurrences in basaltic rocks on the seafloor. Hempton and Savcı (1982) stated that low-degree metabasites of green schist facies are widely exposed around Lake Hazar. The presence of illite and chlorite in core sediments suggests that the lake sediments are derived from the weathering of volcanic rocks exposed in the source area. In fact, illite-chlorite occurrences are recorded in both Maden Group rocks (Daş, 2016) and the Elazığ magmatics (Akkoca et al., 2018) around Lake Hazar.

5.4. Tectonic setting

The major and trace element compositions of clastic sedimentary rocks have been broadly used to identify tectonic settings of the source rocks in a catchment area (Bhatia and Crook, 1986; Roser and Korsch, 1986; Armstrong-Altrin, 2015). Tectonic setting interpretations were carried out using the SiO_2 vs. K_2O/Na_2O diagram of Roser and Korsch (1986). In the SiO_2-K_2O/Na_2O diagram, the lake samples plot within the ARC (volcanic island arc) field (Figure 14a).

Ratios between relatively immobile elements such as Ti, Sc, La, and Zr are considered good indicators of provenance (McLennan et al., 1993). On the La/Sc vs. Ti/Zr diagram (after Bhatia and Crook, 1986) the lake samples plot mainly in the field of oceanic island rocks (Figure 14b). In the La-Sc-Th and Th-Sc-Zr/10 ternary diagrams proposed by Bhatia and Crook (1986), lake samples fall into the oceanic island arc (OIA) field, indicating that source rocks of sediments were formed in an oceanic island setting (Figures 14c and 14d).

Verma and Armstrong-Altrin (2013) suggested two new discriminant diagrams for the tectonic setting of source rocks. These discrimination diagrams were successfully used in recent studies to discriminate the tectonic setting of a source region based on clastic sediment geochemistry (Tawfik et al., 2015; Hernández-Hinojosa et al., 2018). Based on this diagram, the source of four lake samples plots in the collision field, and the remaining samples fall into the arc field (Figure 15). Findings from this diagram are in concordance with the Eastern Tauride subduction model recommended by Robertson et al. (2007). They suggested that arc-related units of the Upper Cretaceous are Elazığ magmatics. According to Yazgan and Chessex (1991), oceanic arc-continent collision occurred during the late Maastrichtian and the Elazığ magmatics (ELM) completed their formation in the Middle Eocene; as a result of arc-related extension, the rocks of the Maden Group (MDG) were formed. A recent study by Ertürk et al. (2018) suggested that Eocene Maden volcanism occurred as a postcollisional product during the extensional collapse of the Southeast Anatolian orogenic belt. Geochemical compositions of lake samples represent the Elazığ magmatic (ELM) and Maden Group (MDG) rocks outcropping in the Kürkçayı River drainage basin and alluvial fans (Figure 16). In the diagram of Bhatia and Crook (1986), Elazığ magmatics and Maden Group samples, which are the source rocks of lake sediments, correspond to an oceanic back arc setting rather than arc-continent collision. However, in the diagram of Verma and Armstrong-Altrin (2013), some samples plot in the collision field.

6. Conclusions

The investigation of the mineralogical and geochemical composition of piston core HZ11-P01 samples from the western margin of Lake Hazar (Eastern Turkey) led to the following findings.

Lake samples are composed of clay minerals (smectite/chlorite mixed-layer clay, chlorite, illite), feldspar, quartz, dolomite, and calcite. The low CIA values of the lake samples indicate a low to moderate degree of alteration of the source rocks. CIW/CIA ratios and ICV values indicate immature detrital material input from bedrocks around the lake area. The C-values suggest mainly semiarid to semihumid climatic conditions over the last 2 ^{14}C ka BP. This is also supported by smectite-chlorite, illite, and chlorite mineral association of clays. Th/U, Ni/

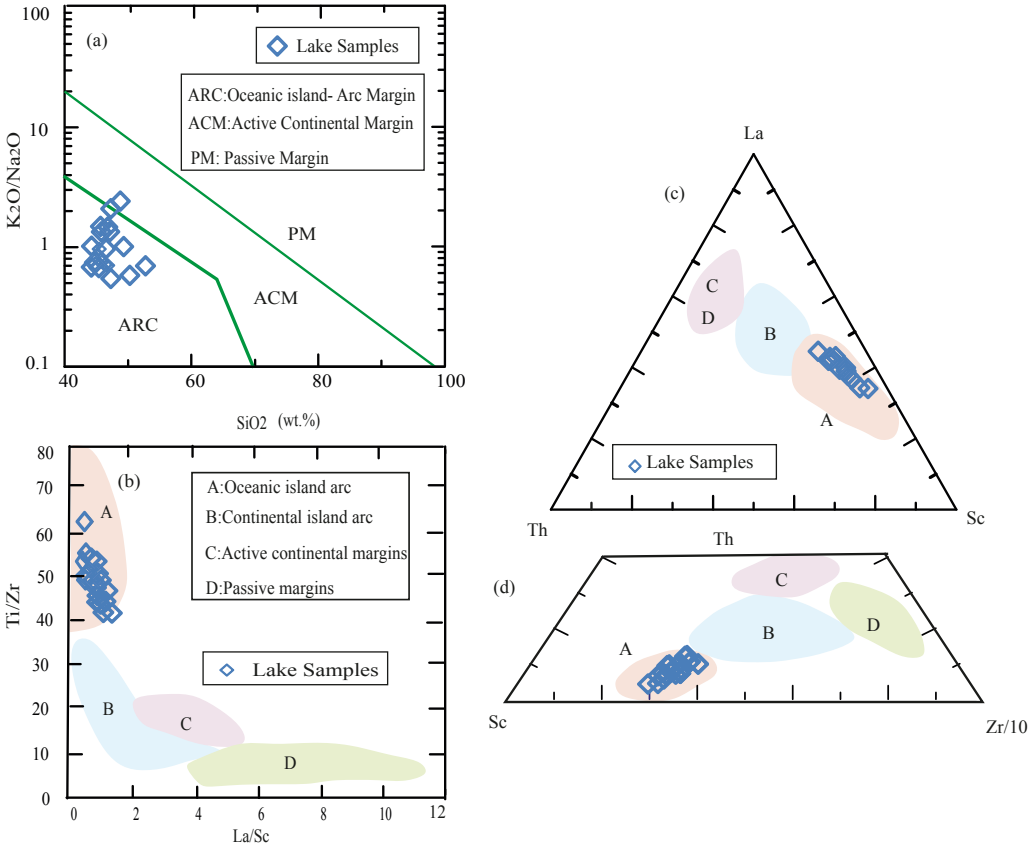

Figure 14. (a) Bivariate plots of SiO_2 vs. (K_2O/Al_2O_3) tectonic discriminant function diagrams (after Roser and Korsch, 1986) for lake samples. (b) La/Sc vs. Ti/Zr plot diagram (after Bhatia and Crook, 1986) for lake samples. (c) Plot of the lake samples in the La-Th-Sc (d) and Th-Sc-Zr/10 diagram reported by Bhatia and Crook (1986). Fields in the diagrams: A = oceanic island arc, B = continental island arc, C = active continental margin, D = passive continental margin.

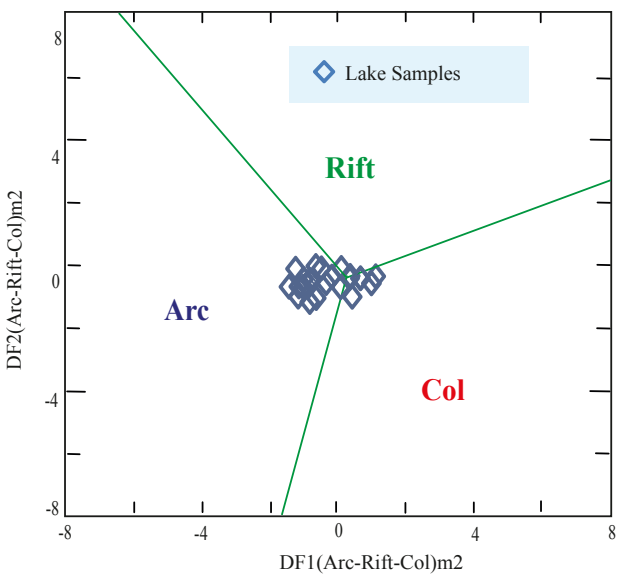

Figure 15. Discriminant-function multidimensional diagram of lake samples for low-silica clastic sediments (from Verma and Armstrong-Altrin, 2013).

Co, Cu/Zn, V/Cr, Eu/Eu*, and Ce/Ce* values reveal the oxic depositional environment in Lake Hazar. The REE patterns, as well as other geochemical parameters such as Eu/Eu*, La/Lu, La/Sc, Th/Sc, La/Co, Th/Co, and Cr/Th elemental ratios of lake samples, support basic to intermediate material in their source rocks. According to the tectonic discrimination diagram, the source rocks of lake samples correspond to arc setting and arc-continent collision fields, consistent with findings of previous studies about the Elazığ magmatics (ELM) and Maden Group (MDG).

Results of whole-rock and clay mineralogical analyses and whole-rock major, trace, and REE analyses of this study are consistent with findings from previous studies. Results of previous mineralogical-petrographic studies showed that the Elazığ magmatics and Maden Group rocks transported to the lake basin have mafic to intermediate composition and formed as a result of arc-continent collision and collision-related extension. Our geochemical data also imply similar results. Previous sedimentological works in the region proposed a cold and

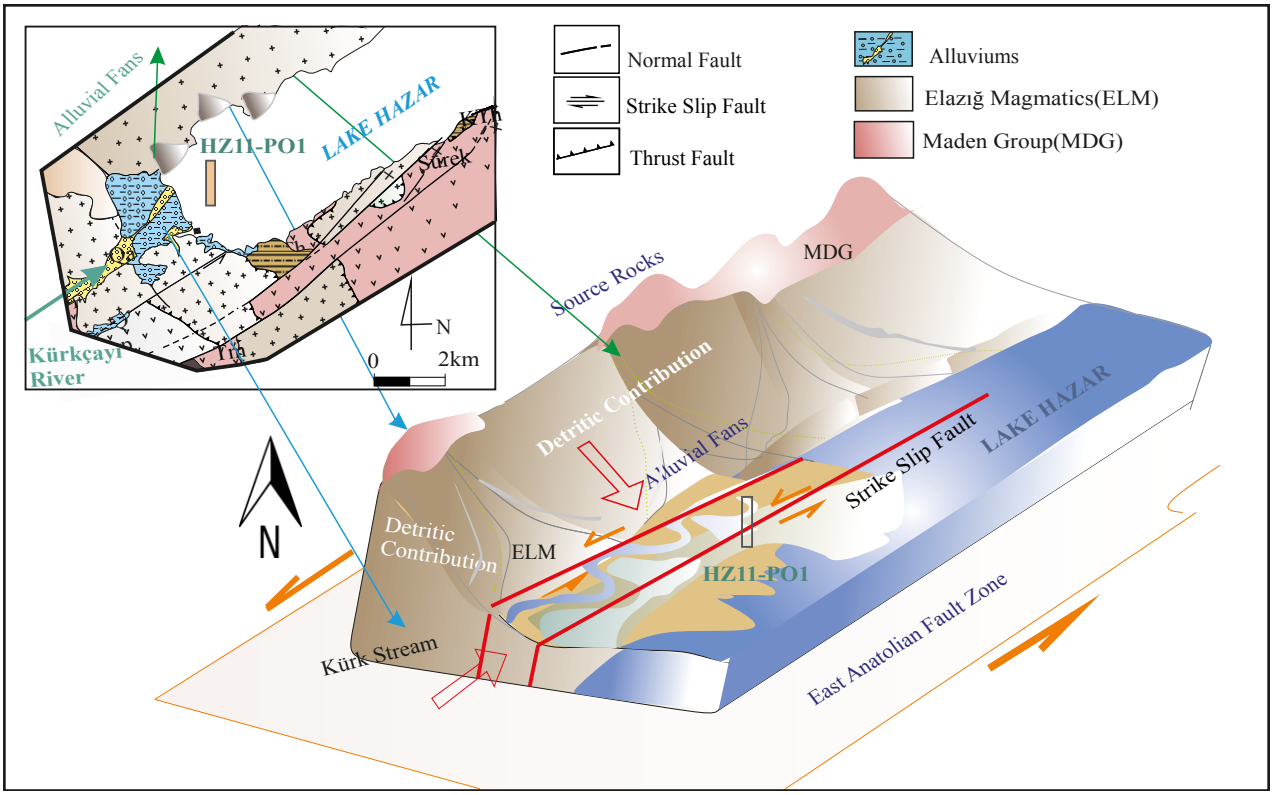

Figure 16. Schematic model showing the western part of Lake Hazar that feeds from the Elazığ magmatics and Maden Group through the Kürkçayı River, and alluvial fans at the drainage basin of the lake.

arid climate regime during 1.4 ^{14}C ka BP, which agrees well with geochemical, whole-rock, and clay mineralogy data on the lake samples of the present study.

Acknowledgments

This study was supported by the Scientific and Technological Research Council of Turkey (TÜBİTAK) under project number 111Y045 and the Fırat University (Turkey) Scientific Research Projects Unit under project number FUBAP-MF 12.07. We also acknowledge the EMCOL Research Center of İstanbul Technical University for allowing the use of field sampling and laboratory facilities for the project. We are grateful to Professor Warren D. Huff, University of Cincinnati, Ohio, USA, for his encouragement and editorial help. Finally, we thank Sena Akçer Ön, Umut Barış Ülgen, Dursun Acar, Emre Damcı, Murat İnceöz, Zülfü Gürocak, and Özlem Öztekin Okan for their great help during fieldwork.

References

Akkoca DB, Işık Ü (2018). Geochemistry of Paleozoic Dadaş Shales from the foreland of Southeastern Turkey, Bismil, Diyarbakır. Periodico di Mineralogia 87: 207-225.

Akkoca DB, Kürüm S, Bakır Z (2018). Mineralogy and geochemical characteristics of Elazığ Magmatics around Yemişlik (East of Elazığ). Science and Engineering Journal of Firat University 30 (2): 87-102.

Aksoy E, İnceöz M, Koçyigit A (2007). Lake Hazar Basin: a negative flower structure on the East Anatolian fault system (EAFS), SE Turkey. Turkish Journal of Earth Sciences 16: 319-338.

Alizai A, Hillier S, Clift PD, Giosan L, Hurst A et al. (2012). Clay mineral variations in Holocene terrestrial sediments from the Indus Basin. Quaternary Research 77: 368-381.

Alt JC, Honnorez J, Laverne C, Emmermann R (1986). Hydrothermal alteration of a 1 km section through the upper oceanic crust, deep sea drilling project hole 504B: mineralogy, chemistry, and evolution of seawater-basalt interactions. Journal of Geophysical Research 91 (10): 309-335.

Armstrong-Altrin JS (2015). Evaluation of two multidimensional discrimination diagrams from beach and deep-sea sediments from the Gulf of Mexico and their application to Precambrian clastic sedimentary rocks. International Geology Review 57: 1446-1461.

Armstrong-Altrin JS, Lee YI, Kasper-Zubillaga JJ, Carranza-Edwards A (2012). Geochemistry of beach sands along the western Gulf of Mexico, Mexico: implication for provenance. Chemie der Erde-Geochemistry 72 (4): 345-362.

Armstrong-Altrin JS, Lee YI, Verma SP, Ramasamy S (2004). Geochemistry of sandstones from the Upper Miocene Kudankulam Formation, southern India: implications for provenance, weathering, and tectonic setting. Journal of Sedimentary Research 74: 285-297.

Armstrong-Altrin JS, Nagarajan R, Madhavaraju J, Rosalez-Hoz L, Lee YI et al. (2013). Geochemistry of the Jurassic and upper Cretaceous shales from the Molango Region, Hidalgo, Eastern Mexico: implications of source-area weathering, provenance, and tectonic setting. Comptes Rendus Geoscience 345: 185-202.

Bhatia MR, Crook K (1986). Trace element characteristics of graywackes and tectonic setting discrimination of sedimentary basins. Contributions to Mineralogy and Petrology 92: 181-193.

Biltekin D, Eriş KK, Çağatay MN, Akçer Ön S, Akkoca Bal D (2018). Late Pleistocene-Holocene environmental change in eastern Turkey: multi-proxy palaeoecological data of vegetation and lake-catchment changes. Journal of Quaternary Science 33 (5): 575-585.

Bingöl AF (1986). Petrographic and petrological characteristics of intrusive rocks of Guleman ophiolite (Eastern Taurus-Turkey). Geosound 13 (4): 41-57.

Bock B, McLennan SM, Hanson GN (1998). Geochemistry and provenance of the Middle Ordovician Ostin Glen Member (Normanskill Formation) and the Taconian orogeny in New England. Sedimentology 45: 635-655.

Bockheim J, Walker DA, Everett LR, Nelson FE, Shiklomanov N (1998). Soils and cryoturbation in moist nonacidic and acidic tundra in the Kuparuk River Basin, Arctic Alaska, U.S.A. Arctic and Alpine Research 30: 166-174.

Bozkaya Ö, Yalçın H, Dündar MK (2006). Relationships between diagenesis/metamorphism and geotectonic setting in the rocks of Maden Group (Malatya-Pütürge). Bulletin of Faculty of Engineering of Cumhuriyet University, Serie A – Earth Sciences 23: 1-24 (in Turkish).

Brindley GW (1980). Chemical compositions of berthierines. A review. Clays and Clay Minerals 30: 153-155.

Çelik H (2003). Stratigraphic and tectonic features of vicinity of Mastar Mountain (SE of Elazığ). PhD, Firat University, Elazığ, Turkey (in Turkish).

Çetin H, Güneyli H, Mayer L (2003). Palaeoseismology of the Palu-Lake Hazar segment of the East Anatolian Fault Zone, Turkey. Tectonophysics 374: 163-197.

Chamley H (1989). Clay Sedimentology. Berlin, Germany: Springer Verlag.

Condie KC, Marais DJD, Abbott D (2001). Precambrian superplumes and supercontinents: a record in black shales, carbon isotopes, and paleoclimates. Precambrian Research 106: 239-260.

Coppin F, Berger G, Bauer A, Castet S, Loubet M (2002). Sorption of lanthanides on smectite and kaolinite. Chemical Geology 182: 57-68.

Cox R, Lowe DR, Cullers R (1995). A conceptual review of regional-scale controls on the composition of clastic sediment and the co-evolution of continental blocks and their sediment cover. Journal of Sedimentary Research 1: 1-12.

Craigie N (2018). Principles of Elemental Chemostratigraphy. Cham, Switzerland: Springer International Publishing AG.

Cullers RL (1994). The controls on major and trace element variation of shales, siltstones, and sandstones of Pennsylvanian-Permian age from uplifted continental blocks in Colorado to platform sediment in Kansas, USA. Geochimicia et Cosmochimicia Acta 58: 4955-4972.

Cullers RL (1995). The controls on the major and trace element evolution of shales, siltstones and sandstones of Ordovician to Tertiary age in the Wet Mountain region, Colorado, U.S.A. Chemical Geology 123: 107-131.

Cullers RL (2002). The geochemistry of shales, siltstones and sandstones of Pennsylvanian-Permian age, Colorado, USA: implications for provenance and metamorphic studies. Lithos 51: 181-203.

Cullers RL, Basu A, Suttner L (1988). Geochemical signature of provenance in sand - size material in soils and river sediments near the Tobacco Root batholith, Montana, USA. Chemical Geology 70: 335-348.

Cullers RL, Berendsen P (1998). The provenance and chemical variation of sandstones associated with the Mid-Continent Rift system, USA. European Journal of Mineralogy 10: 987-1002.

Cullers RL, Graf J (1983). Rare earth elements in igneous rocks of the continental crust: intermediate and silicic rocks, ore petrogenesis. In: Henderson P (editor). Rare-Earth Geochemistry. Amsterdam, the Netherlands: Elsevier, pp. 275-312.

Cullers RL, Podkovyrov VN (2000). Geochemistry of the Mesoproterozoic Lakhanda shales in southeastern Yakutia, Russia: implications for mineralogical and provenance control, and recycling. Precambrian Research 104: 77-93.

Dabard MP (1990). Lower Broverian formations (Upper Proterozoic) of the Armorican Massif (France): geodynamic evolution of source areas revealed by sandstone petrography and geochemistry. Sedimentary Geology 69: 45-58.

Daş B (2016). Clay mineralogy and geochemical properties of marine sedimentary and volcanosedimentary rocks at the vicinity of Hatunköy-Plajköy (southeast of Elazığ). MSc thesis, Firat University, Elazığ, Turkey (in Turkish).

Descourvieres C, Douglas G, Leyland L, Hartog N, Prommer H (2011). Geochemical reconstruction of the provenance, weathering and deposition of detrital-dominated sediments in the Perth Basin: the Cretaceous Leederville Formation, south-west Australia. Sedimentary Geology 236: 62-76.

Dill H (1986). Metallogenesis of Early Paleozoic graptolite shales from the Graefenthal Horst northern Bavaria-Federal Republic of Germany. Economic Geology 81: 889-903.

Dix G (2006). Origin of anhedral Sr-rich calcite in deep-water mixed sediment, north-east Australia, Sedimentology 42 (5): 711-724.

Dönmez C (2006). Geology, petrography and geochemistry of the Elazığ Magmatics outcropping between Soğanlı-Uyandık (Elazığ). MSc, Çukurova University, Adana, Turkey (in Turkish).

Dypvik H (1984). Geochemical compositions and depositional conditions of Upper Jurassic and Lower Cretaceous Yorkshire clays, England. Geological Magazine 121: 489-504.

Eker SÇ (2012). Petrography and geochemistry of Eocene sandstones from eastern Pontides (NE Turkey): implications for source area weathering, provenance and tectonic setting. Geochemistry International 50 (8): 683-701.

Eker SÇ, Korkmaz S (2011). Mineralogy and whole rock geochemistry of Late Cretaceous sandstones from the Eastern Pontides, (NE Turkey). Neues Jahrbuch für Mineralogie Abhandlungen 188: 235-256.

Erdem E (1987). Petrological investigation of magmatic rocks around Elazığ Kartaldere Gölardı (NE of Hazar Lake). MSc, Fırat University, Elazığ, Turkey (in Turkish).

Eriş KK (2013). Late Pleistocene Holocene sedimentary records of climate and lake- level changes in Lake Hazar, Eastern Anatolia, Turkey. Quaternary International 302: 123-134.

Eriş KK, Arslan TN, Sabuncu A (2018b). Influences of climate and tectonic on the middle to late Holocene deltaic sedimentation in Lake Hazar, Eastern Turkey. Arabian Journal for Science and Engineering 43: 3685-3697.

Eriş KK, Ön SA, Çagatay MN¸ Ülgen UB, Ön ZB et al. (2018a). Late Pleistocene to Holocene paleoenvironmental evolution of Lake Hazar, Eastern Anatolia, Turkey. Quaternary International 436: 4-16.

Ertürk MA, Beyarslan M, Chung SL, Lin TH (2018). Eocene magmatism (Maden Complex) in the Southeast Anatolian Orogenic Belt: magma genesis and tectonic implications. Geoscience Frontiers 9 (6): 1829-1847.

Fedo CM, Eriksson K, Krogstad EJ (1996). Geochemistry of shale from the Archean (~3.0 Ga) Buhwa Greenstone belt, Zimbabwe: implications for provenance and source area weathering. Geochimica Cosmochimica Acta 60: 1751-1763.

Fedo CM, Nesbitt HW, Young GM (1995). Unravelling the effects of potassium metasomatism in sedimentary rocks and paleosols, with implications for paleoweathering conditions and provenance. Geology 23: 921-924.

Fischer G, Wefer G (1999). Use of Proxies in Paleoceanography: Examples from the South Atlantic. New York, NY, USA: Springer-Verlag.

Floyd PA, Winchester JA, Park RG (1989). Geochemistry and tectonic setting of Lewisian clastic metasediments from the early Proterozoic Loch Maree Group of Gairloch, NW Scotland. Precambrian Research 45: 203-214.

Folk RL (1974). Petrology of Sedimentary Rocks. Austin, TX, USA: Hemphill Publishing Company.

Gao S, Wedepohl KH (1995). The negative Eu anomaly in Archean sedimentary rock: implications for decomposition, age and importance of their granitic sources. Earth and Planetary Science Letters 133: 81-94.

Garcia-Moreno D, Hubert A, Moernaut J, Fraser J, Boes X et al. (2010). Structure and evolution of Lake Hazar pull-apart basin along the East Anatolian Fault. Basin Research 36: 191-207.

Garzanti E, Al-Juboury AI, Zoleikhaei Y, Vermeesch P, Jaafar J et al. (2016). The Euphrates-Tigris-Karun River system: provenance, recycling and dispersal of quartz-poor foreland-basin sediments in arid climate. Earth Science Reviews 162: 107-128.

Gromet LP, Dymek RF, Haskin LA, Korotev RI (1984). The North American Shale Composite: its compilation, major and trace element characteristics. Geochimica et Cosmochimicia Acta 48: 2469-2482.

Guo Q, Shields GA, Liu C, Strauss H, Zhu M et al. (2007). Trace element chemostratigraphy of two Ediacaran-Cambrian successions in South China: implications for organosedimentary metal enrichment and silicification in the early Cambrian. Palaeogeography, Palaeoclimatology, Palaeoecology 254: 194-216.

Gürocak Z (1993). Geology of Sivrice town (Elazığ). MSc, Firat University, Elazığ, Turkey (in Turkish).

Hallberg RO (1976). A geochemical method for investigation of paleoredox conditions in sediments. Ambio Special Report 4: 139-147.

Hara H, Kurihara T, Kuroda J, Adach Y, Kurita H et al. (2010). Geological and geochemical aspects of a Devonian siliceous succession in northern Thailand: implications for the opening of the Paleo-Tethys. Palaeogeography, Palaeoclimatology, Palaeoecology 297: 452-464.

Harnois L (1988). The CIW index: a new chemical index of weathering. Sedimentary Geology 55: 319-322.

Hempton MR, Dunne LA, Dewey JF (1983). Sedimentation in active strike-slip basin, Southeastern Turkey. Journal of Geology 91: 401-412.

Hempton MR, Savcı G (1982). Petrological and structural features of the Elazığ volcanic complex. Türkiye Jeoloji Kurumu Bülteni 25: 143-151 (in Turkish).

Hernández-Hinojosa V, Montiel-García PC, Armstrong-Altrin JS, Nagarajan R, Kasper-Zubillaga JJ (2018). Textural and geochemical characteristics of beach sands along the western Gulf of Mexico, Mexico. Carpathian Journal of Earth and Environmental Sciences 13: 161-174.

Herron MM (1988). Geochemical classification of terrigenous sands and shales from core or log data. Journal of Sedimentary Research 58: 820-825.

Hseu ZY, Tsai H, His HC, Chen YC (2007). Weathering sequences of clay minerals in soils along a serpentinitic toposequence. Clays and Clay Minerals 55 (4): 389-401.

Huvaj YN, Huff WD (2016). Clay mineralogy and geochemistry of three offshore wells in the southwestern Black Sea, northern Turkey: the effect of burial diagenesis on the conversion of smectite to illite. Turkish Journal of Earth Sciences 25: 592-610.

Johnsson MJ (2000). Tectonic assembly of east-central Alaska: evidence from Cretaceous-Tertiary sandstones of the Kandik River terrane. Geological Society of America Bulletin 112: 1023-1042.

Jones B, Manning DAC (1994). Comparison of geological indices used for the interpretation of palaeoredox conditions in ancient mudstones. Chemical Geology 111: 111-129.

Khalifa A, Çakır Z, Owen LA, Kaya Ş (2018). Morphotectonic analysis of the East Anatolian Fault, Turkey. Turkish Journal of Earth Sciences 27: 110-126.

Kimura H, Watanabe Y (2001). Oceanic anoxia at the Precambrian-Cambrian boundary. Geology 29: 995-998.

Kiseeva ES, Fonseca ROC, Smythe DJ (2017). Chalcophile elements and sulfides in the upper mantle. Elements 13: 111-116.

Ling HF, Chen X, Li DA, Wang D, Shields-Zhou GA et al. (2013). Cerium anomaly variations in Ediacaran–earliest Cambrian carbonates from the Yangtze Gorges area, South China: implications for oxygenation of coeval shallow seawater. Precambrian Research 225: 1-18.

Liu W, Huang Y, An Z, Clemens SC, Li L et al. (2005). Summer monsoon intensity controls C4/C3 plant abundance during the last 35 ka in the Chinese Loess Plateau; carbon isotope evidence from bulk organic matter and individual leaf waxes. Palaeogeography, Palaeoclimatology, Palaeoecology 220 (3/4): 243-254.

Malick BML, Ishiga H (2016). Geochemical classification ad determination of maturity source weathering in beach sands of eastern San'in Coast, Tango Peninsula, and Wakas Bay, Japan. Earth Science Research 5: 44-56.

Martinez-Ruiz F, Kastner M, Gallego-Torres D, Rodrigo-Gamiz M, Nieto-Moreno V et al. (2015). Paleoclimate and paleoceanography over the past 20.000 yr in the Mediterranean Sea Basins as indicated by sediment elemental proxies. Quaternary Science Reviews 107: 25-46.

Maynard JB (1992). Chemistry of modern soils as a guide to interpreting Precambrian paleosols. Journal of Geology 100: 279-289.

McLennan SM (1993). Weathering and global denudation. Journal of Geology 101: 295-303.

McLennan SM (2001). Relationships between the trace element composition of sedimentary rocks and upper continental crust. Geochemistry Geophysics Geosystems 2 (4): 1021-1024.

McLennan SM, Hemming S, McDaniel D, Hanson G (1993). Geochemical approaches to sedimentation, provenance, and tectonics. Geological Society of America Special Papers 284: 21-40.

Millot G (1970). Geology of Clays. New York, NY, USA: Springer.

Milodowsky AE, Zalasiewicz JA (1991). Redistribution of rare-earth elements during diagenesis of turbidite/hemipelagite mudrock sequences of Liandovery age from central Wales. Geological Society of London Special Publications 57: 101-124.

Mir AR (2015). Rare earth element geochemistry of Post- to Neoarchean shales from Singhbhum mobile belt, Eastern India: implications for tectonic setting and paleo-oxidation conditions. Chinese Journal of Geochemistry 34 (3): 401-409.

Mishra M, Sen S (2012). Provenance, tectonic setting and source-area weathering of Mesoproterozoic Kaimur Group, Vindhyan Supergroup, Central India. Geologica Acta 10: 283-293.

Mongelli G, Cullers, RL, Muelheisen S (1996). Geochemistry of Late Cretaceous-Oligocenic shales from the Varicolori Formation, southern Apennines, Italy: implications for mineralogical, grain-size control and provenance. European Journal of Mineralogy 8: 733-754.

Mourabet ME, Barakat A, Zaghloul MN, Baghdadi ME (2018). Geochemistry of the Miocene Zoumi flysch thrust-top basin (External Rif, Morocco): a new constrains on source area weathering, recycling processes, and paleoclimate conditions. Arabian Journal of Geosciences 11 (126): 2-18.

Möller P, Bau M (1993). Rare-earth patterns with positive cerium anomaly in alkaline waters from Lake Van, Turkey. Earth and Planetary Science Letters 117: 671-676.

Nagarajan R, Madhavaraju J, Armstrong-Altrin JS, Nagendra R (2007). Geochemistry of Neoproterozoic limestones of the Shahabad Formation, Bhima Basin, Karnataka, southern India. Journal of Geosciences 15: 9-25.

Nesbitt HW, Young GM (1982). Early Proterozoic climate and plate motions inferred from major element chemistry of lutites. Nature 299: 715-717.

Ön ZB, Ön AS, Ozeren MS, Eriş KK, Greaves MA et al. (2017). Climate proxies for the last 17.3 ka from Lake Hazar (Eastern Anatolia), extracted by independent component analysis of m-XRF data. Quaternary International 486: 17-28.

Rahman MJJ, Suzuki S (2007). Geochemistry of sandstones from the Miocene Surma Group, Bengal Basin, Bangladesh: implications for provenance, tectonic setting and weathering. Geochemical Journal 41: 415-428.

Rimmer SM (2004). Geochemical paleoredox indicators in Devonien-Missipian Black Shales, Central Appalachian Basin (USA). Chemical Geology 206: 373-391.

Robertson AHF, Parlak O, Rizaoglu T, Ünlügenc UC, Inan N et al. (2007). Tectonic evolution of the South Tethyan Ocean: evidence from the Eastern Taurus Mountains (Elazig region, SE Turkey). In: Ries AC, Butler RWH, Graham RH (editors). Deformation of the Continental Crust. The Legacy of Mike Coward. London, UK: Geological Society of London Special Publications, pp. 231-270.

Roddaz M, Viers J, Brusset S, Baby P, Boucayrand C et al. (2006). Controls on weathering and provenance in the Amazonian foreland basin: insights from major and trace element geochemistry of Neogene Amazonian sediments. Chemical Geology 226: 31-65.

Roser BP, Korsch RJ (1986). Determination of tectonic setting of sandstone-mudstone suites using SiO_2 content and K_2O/Na_2O ratio. Journal of Geology 94 (5): 635-650.

Şengör AMC, Görür N, Saroğlu F (1985). Strike-slip faulting and related basin formation in zones of tectonic escape: Turkey as a case study. Society for Sedimentary Geology 37: 227-267.

Şengün F, Koralay OE (2019). Petrography, geochemistry, and provenance of Jurassic sandstones from the Sakarya Zone, NW Turkey. Turkish Journal of Earth Sciences 28: 603-622.

Shields G, Stille P (2001). Diagenetic constrains on the use of cerium anomalies as palaeoseawater redox proxies: an isotopic and REE study of Cambrian phosphorites. Chemical Geology 175: 29-48.

Sholkovitz ER (1988). Rare earth elements in the sediments of the North Atlantic Ocean, Amazon delta and East China Sea: reinterpretation of terrigenous input patterns to the ocean. Journal of American Science 288: 236-228.

Siani G, Paterne M, Arnold M, Bard E, Metivier B et al. (2000). Radiocarbon reservoir ages in the Mediterranean Sea and Black Sea. Radiocarbon 42: 271-280.

Song E, Zhang K, Chen J, Wang C, Jiang G et al. (2014). Clay mineralogy and its paleoclimatic significance of the Oligocene-Miocene sediments in the Gerze Basin, Tibet. Acta Geologica Sinica 88 (5): 1579-1591.

Stuiver M, Reimer PJ (1993). Extended 14 C database and revised CALIB radiocarbon calibration program. Radiocarbon 35: 215-230.

Tang Y, Sang L, Yuan Y, Zhang Y, Yang Y (2012). Geochemistry of Late Triassic pelitic rocks in the NE part of Songpan-Ganzi Basin, western China: implications for source weathering, provenance and tectonic setting. China University of Geosciences (Beijing) Geoscience Frontiers 3 (5): 647-660.

Tao H, Wang Q, Yang X, Jiang L (2013). Provenance and tectonic setting of Late Carboniferous clastic rocks in West Junggar, Xinjiang, China: a case from the Hala-alat Mountains. Journal of Asian Earth Sciences 64: 210-222.

Tawfik HA, Ghandou IM, Maejima W, Armstrong-Altrin JS, Abdel-Hameed AT (2015). Petrography and geochemistry of the siliciclastic Araba Formation (Cambrian), east Sinai, Egypt: implications for provenance, tectonic setting and source weathering. Geological Magazine 154: 1-23.

Taylor SR, McLennan SM (1985). The Continental Crust: Its Composition and Evolution. 1st ed. Oxford, UK: Blackwell.

Temel A, Gündoğdu MN (1996). Zeolite occurrences and the erionite-mesothelioma relationship in Cappadocia, Central Anatolia, Turkey. Mineraleum Deposita 31: 539-547.

Tetiker S (2014). Petrography and geochemistry of early Palaeozoic clastic rocks from the southeast Anatolian autochthone rocks in Mardin area (Derik-Kızıltepe), Turkey. Carpathian Journal of Earth and Environmental Sciences 1: 149-162.

Toulkeridis T, Clauer N, Kröner A, Reimer T, Todt W (1999). Characterization, provenance, and tectonic setting of fig tree greywackes from the Archaen Barberton greenstone belt, South Africa. Sedimentary Geology 124: 113-129.

Tribovillard N, Algeo TJ, Lyons T, Riboulleau A (2006). Trace metals as paleoredox and paleoproductivity proxies: an update. Chemical Geology 232: 12-32.

Uddin MK (2017). A review on the adsorption of heavy metals by clay minerals, with special focus on the past decade. Chemical Engineering Journal 308: 438-462.

Ural M, Arslan M, Göncüoğlu MC, Tekin UK, Kürüm S (2015). Late cretaceous arc and back-arc formation within the southern Neotethys: whole-rock, trace element and Sr-Nd-Pb isotopic data from basaltic rocks of the Yüksekova Complex (Malatya-Elazığ, SE Turey). Ofioliti 4: 57-72.

Verma SP, Armstrong-Altrin JS (2013). New multi-dimensional diagrams for tectonic discrimination of siliclastic sediments and their application to Precambrian basins. Chemical Geology 355: 117-133.

Vital H, Stattegger K (2000). Major and trace elements of stream sediments from the lowermost Amazon River. Chemical Geology 168: 151-168.

Wanas HA, Abdel-Maguid NM (2006). Petrography and geochemistry of the Cambro-Ordovician Wajid Sandstone, southwest Saudi Arabia: implications for provenance and tectonic setting. Journal of Asian Earth Sciences 27 (4): 416-429.

Wedepohl KH (editor) (1978). Handbook of Geochemistry II/2. Berlin, Germany: Springer.

Wignall PB, Myers KJ (1988). Interpreting benthic oxygen levels in mudrocks: a new approach. Geology 16 (5): 452-455.

Wignall PB, Twitchett RJ (1996). Ocean anoxia and the end-Permian mass extinction. Science 272: 1155-1S158.

Yang K, Kim JW, Kogure T, Dong H, Baik H et al. (2016). Smectite, illite, and early diagenesis in South Pacific Gyre subseafloor sediment. Applied Clay Science 134: 34-43.

Yang Z, Lu W, Bao X, Yang Q (2011). Assessment of heavy metal contamination in urban topsoil from Changchun City, China. Journal of Geochemistry Exploration 108: 27-38.

Yazgan E, Chessex R (1991). Geology and tectonic evolution of the southeastern Taurides in the region of Malatya. *Turkish Association* of *Petroleum* Geologists 3: 1-42.

Yuretich R, Melles M, Sarata B, Grobe H (1999). Clay minerals in the sediments of Lake Baikal: a useful climate proxy. Journal of Sedimentary Research 69 (3): 588-596.

Zhao Z, Zhao, JH, Wang HJ, Liao JD, Liu CM (2007). Distribution characteristics and applications of trace elements in Junggar Basin. Natural Gas Exploration and Development 30: 30-33.